J|A|C|S ARTICLES

Published on Web 02/03/2010

Catalyst-Site-Controlled Coordination Polymerization of Polar Vinyl Monomers to Highly Syndiotactic Polymers

Yuetao Zhang,[†] Yalan Ning,[†] Lucia Caporaso,[‡] Luigi Cavallo,*[,‡] and Eugene Y.-X. Chen*[,†]

Department of Chemistry, Colorado State University, Fort Collins, Colorado 80523-1872, and Dipartimento di Chimica, Università di Salerno, Via Ponte don Melillo, I-84084 Fisciano (SA), Italy

Received October 15, 2009; E-mail: lcavallo@unisa.it; eugene.chen@colostate.edu

Abstract: This contribution reports a combined synthetic, kinetic, mechanistic, and theoretical/computational study of the recently discovered catalyst-site-controlled coordination polymerization of polar vinyl monomers [such as methyl methacrylate (MMA) and *N*,*N*-dimethylacrylamide (DMAA)] into highly syndiotactic polymers. Among the 12 C_s-ligated *ansa*-cyclopentadienyl (Cp)-R_2E(C,Si)-fluorenyl (Flu) group 4 metallocene catalyst systems examined—which varied in metal center, anion structure, bridging atom and substituents, and ligand substitution pattern—cationic *ansa*-metallocene ester enolate catalyst **6**$^+[B(C_6F_5)_4]^-$, derived from the activation of the precatalyst [Ph_2C(Cp)(2,7-^{t}Bu$_2$-Flu)]Zr[OC(O^{i}Pr)=CMe_2]$_2$ with [Ph_3C][$B(C_6F_5)_4$], stood out as the best catalyst in *all* aspects of the MMA polymerization at room temperature, including the highest activity (1554 h^{-1} TOF), efficiency (98% *I**), syndiotacticity (94% *rr*), and control (predicted number-average molecular weight and 1.14 molecular weight distribution). Kinetic and mechanistic results are consistent with a catalyst-site-controlled, monometallic coordination−addition mechanism, involving fast intramolecular addition within the catalyst−monomer complex leading to the resting eight-membered ester enolate chelate, followed by the rate-limiting ring-opening of the chelate to regenerate the active species. This work has also uncovered several unique features of this polymerization system that are in marked contrast to the propylene polymerization by analogous C_s-ligated cationic alkyl catalysts: a constant syndiotacticity of PMMA produced over a wide polymerization temperature range (i.e., from 0 °C, 94% *rr* to 25 °C, 94% *rr* to 50 °C, 93% *rr*); insensitivity of its high activity, degree of control, and stereoselectivity to solvent polarity and structure of weakly coordinating anions; and deviation from a pure site-control mechanism at high [MMA]/[catalyst] ratios. Computational results provide theoretical support for the proposed monomer-assisted, catalyst-site epimerization, after an enantiofacial mistake, to a thermodynamically more stable resting state, which accounts for the observed higher than expected [*mr*] contents based on a pure site-controlled mechanism. DFT calculations rationalize why the $Ph_2C<$ bridged catalyst **6** exhibits higher stereoselectivity than other catalysts with the $Me_2C<$ or $Me_2Si<$ bridge: the bridge rigidity pushes the η^3-bound Flu ligand closer to the growing chain and the monomer, thereby increasing ΔE_{stereo} between the competing transition states for the addition of a monomer molecule to the opposite (correct and wrong) enantiofaces of the enolate growing chain. The relative polymerization activity of this catalyst series is shown to correlate with the relative energetics of the back-biting of the penultimate unit and ion-pair formation.

Introduction

Coordination polymerization of polar vinyl monomers by single-site metal catalysts,[1] especially those of cationic group 4 metallocene catalysts,[2] which have been extensively investigated for the (co)polymerization of nonpolar vinyl monomers (α-olefins in particular),[3] has attracted increasing interest due to its precision in catalyst-based stereochemical and architectural control as well as its ability to produce new classes of polymeric

[†] Colorado State University.
[‡] Università di Salerno.

(1) Chen, E. Y.-X. *Chem. Rev.* **2009**, *109*, 5157–5214.

(2) Selected reference works and reviews: (a) Chen, E. Y.-X.; Rodriguez-Delgado, A. Complexes of Zirconium and Hafnium in Oxidation State IV In *Comprehensive Organometallic Chemistry III*; Bochmann, M., Vol. Ed., Mingos, M. P., Crabtree, R. H., Chief Eds.; Elsevier: Oxford, 2007; Vol. *4*, pp 759−1004. (b) Cuenca, T. In Complexes of Titanium in Oxidation State IV. In *Comprehensive Organometallic Chemistry III*; Bochmann, M., Vol. Ed., Mingos, M. P., Crabtree, R. H., Chief Eds.; Elsevier: Oxford, 2007; Vol*4*, pp 323−696, (c) Bochmann, M. *J. Chem. Soc., Dalton Trans.* **1996**, 255–270. (d) Jordan, R. F. *Adv. Organomet. Chem.* **1991**, *32*, 325–387.

(3) Selected books, reference works, or journal reviews: (a) *Stereoselective Polymerization with Single-Site Catalysts*; Baugh, L. S., Canich, J. A. M., Eds.; CRC Press: Boca Raton, FL, 2008. (b) Resconi, L.; Chadwick, J. C.; Cavallo, L. Olefin Polymerizations with Group IV Metal Catalysts In *Comprehensive Organometallic Chemistry III*; Bochmann, M., Vol. Ed., Mingos, M. P., Crabtree, R. H., Chief Eds.; Elsevier: Oxford, 2007; Vol*4*, pp 1005−1166. (c) Domski, G. J.; Rose, J. M.; Coates, G. W.; Bolig, A. D.; Brookhart, M. *Prog. Polym. Sci.* **2007**, *32*, 30–92. (d) Marks, T. J., Ed. *Proc. Natl. Acad. Sci. U.S.A.* **2006**, *103*, 15288−15354 and contributions therein (issue on Polymerization Special Feature). (e) Gibson, V. C.; Spitzmesser, S. K. *Chem. Rev.* **2003**, *103*, 283–315. (f) Gladysz, J. A., Ed *Chem. Rev.* **2000**, *100*, 1167−1681 and contributions therein (issue on Frontiers in Metal-Catalyzed Polymerization). (g) Brintzinger, H. H.; Fischer, D.; Mülhaupt, R.; Rieger, B.; Waymouth, R. M. *Angew. Chem., Int. Ed.* **1995**, *34*, 1143–1170.

Scheme 1. Elementary Steps Involved in Coordination−Addition Polymerization of Methyl Methacrylate[a]

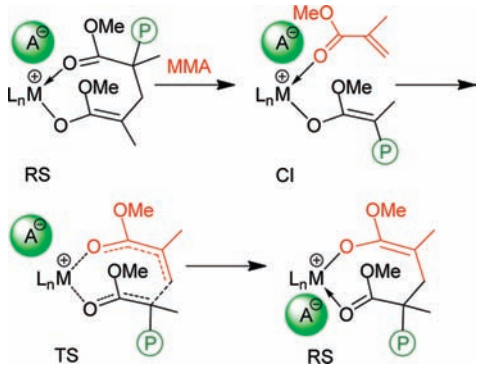

[a] Abbreviations: RS, resting state; CI, coordination intermediate; TS, transition state; L_n, supporting ligand; M, metal; A, anion; and P, growing polymer chain.

materials unattainable by other means of polymerization.[1] In this context, remarkable successes have been achieved in both metal-catalyzed coordination−addition and coordination−insertion polymerizations of polar vinyl monomers. On one hand, *coordination−addition* polymerization of polar vinyl monomers (Scheme 1) by single-site early metal and lanthanide catalysts can generate a dazzling variety of stereomicrostructures, in addition to its high activity and high degree of control over polymerization characteristics. On the other hand, *coordination−insertion* copolymerization of α-olefins with polar vinyl monomers by late metal catalysts demonstrates tantalizing versatility, incorporating a wide range of polar vinyl monomers at controllable levels into polyolefins with diverse topologies.[1]

Mechanistic studies of the methyl methacrylate (MMA) polymerization catalyzed by various types of group 4 cationic metallocene complexes, including those supported by C_2-,[4] C_{2v}-,[5] C_1-,[6] and constrained geometry catalyst[7] (C_s)-ligated catalysts, have revealed important insights into polymerization kinetics, fundamental steps (initiation, propagation, and termination/side reactions), and stereocontrol events. Theoretical/computational investigations[8] provide a synergistic understanding of such polymerization reactions, especially aspects of stereocontrol mechanisms[7a,8a,c] in the MMA polymerization by chiral *ansa*-zirconocenium complexes. Most notable in terms of a high degree of control in both polymerization and stereoregulation are chiral C_2-ligated zirconocenium catalysts, such as {*rac*-(EBI)Zr(THF)[OC(O^{i}Pr)=CMe$_2$]}$^+$[MeB(C$_6$F$_5$)$_3$]$^-$ [EBI = C$_2$H$_4$(η^5-indenyl)$_2$],[4] that can readily produce highly isotactic (*it*-) polymethacrylates (≥95% *mm*)[4,9] and polymethacrylamides (>99% *mm*).[10]

In marked contrast, attempts by at least five research groups[6c,9a,11] over the past decade to synthesize highly syndiotactic polymethacrylates such as syndiotactic poly(methyl methacrylate) [*st*-PMMA, a technologically more important material than its *it*-counterpart due to its much higher (~85 °C) glass-transition temperature (T_g)[1]], using the prototype C_s-ligated cationic zirconocene methyl complex [Me$_2$C(Cp)(Flu)ZrMe]$^+$ (Cp = η^5-cyclopentadienyl; Flu = η^3-fluorenyl), have been unsuccessful. Such C_s-ligated catalysts are well-known for their ability to catalyze the syndiospecific polymerization of propylene,[12] but the use of [Me$_2$C(Cp)(Flu)]ZrMe$_2$, upon activation with various activators including B(C$_6$F$_5$)$_3$,[9a] [^{n}Bu$_3$NH][BPh$_4$],[6c] [Ph$_3$C][B(C$_6$F$_5$)$_4$]/Et$_2$Zn (excess),[11c] and B(C$_{12}$F$_9$)$_3$,[11b] as well as the use of the isolated cationic species [Me$_2$C(Cp)(Flu)]Zr(Me)MeB(C$_6$F$_5$)$_3$ (**1**),[11a] yielded no polymer formation. Although this inactivity issue was later solved by using an ester enolate derivative, {Me$_2$C(Cp)(Flu)Zr(THF)[OC(O^{i}Pr)=CMe$_2$]}$^+$[MeB(C$_6$F$_5$)$_3$]$^-$ (**2**),[13] which simulates the proposed active propagating species, the PMMA produced at room temperature is a syndio-rich atactic polymer (64% *rr*, 32% *mr*, 4.0% *mm*) formed via an apparent chain-end control mechanism [as a methyl triad test using 4[*mm*][*rr*]/[*mr*]^2 gave 1.0] rather than the site-controlled mechanism expected on the basis of the propylene polymerization precedent.

This quest has also been extended to lanthanide hydrocarbyls or amides incorporating C_s-symmetric *ansa*-Cp-9-Flu ligands, including Me$_2$C< bridged yttrocene, [Me$_2$C(Cp)(Flu)]Y(THF)CH(SiMe$_3$)$_2$;[14] Ph$_2$C< bridged lutetocene, [Ph$_2$C(Cp)(Flu)]LuN(SiMe$_3$)$_2$;[15] Me$_2$Si< bridged yttrocene,

(4) (a) Rodriguez-Delgado, A.; Chen, E. Y.-X. *Macromolecules* **2005**, *38*, 2587–2594. (b) Bolig, A. D.; Chen, E. Y.-X. *J. Am. Chem. Soc.* **2004**, *126*, 4897–4906.
(5) (a) Ning, Y.; Cooney, M. J.; Chen, E. Y.-X. *J. Organomet. Chem.* **2005**, *690*, 6263–6270. (b) Stojcevic, G.; Kim, H.; Taylor, N. J.; Marder, T. B.; Collins, S. *Angew. Chem., Int. Ed.* **2004**, *43*, 5523–5526. (c) Lian, B.; Toupet, L.; Carpentier, J.-F. *Chem.—Eur. J.* **2004**, *10*, 4301–4307. (d) Bandermann, F.; Ferenz, M.; Sustmann, R.; Sicking, W. *Macromol. Symp.* **2001**, *174*, 247–253. (e) Li, Y.; Ward, D. G.; Reddy, S. S.; Collins, S. *Macromolecules* **1997**, *30*, 1875–1883.
(6) (a) Strauch, J. W.; Fauré, J.-L.; Bredeau, S.; Wang, C.; Kehr, G.; Fröhlich, R.; Luftmann, H.; Erker, G. *J. Am. Chem. Soc.* **2004**, *126*, 2089–2104. (b) Jin, J.; Mariott, W. R.; Chen, E. Y.-X. *J. Polym. Chem. Part A: Polym. Chem.* **2003**, *41*, 3132–3142. (c) Frauenrath, H.; Keul, H.; Höcker, H. *Macromolecules* **2001**, *34*, 14–19.
(7) (a) Ning, Y.; Caporaso, L.; Correa, A.; Gustafson, L. O.; Cavallo, L.; Chen, E. Y.-X. *Macromolecules* **2008**, *41*, 6910–6919. (b) Lian, B.; Thomas, C. M.; Navarro, C.; Carpentier, J.-F. *Organometallics* **2007**, *26*, 187–195. (c) Rodriguez-Delgado, A.; Mariott, W. R.; Chen, E. Y.-X. *Macromolecules* **2004**, *37*, 3092–3100. (d) Nguyen, H.; Jarvis, A. P.; Lesley, M. J. G.; Kelly, W. M.; Reddy, S. S.; Taylor, N. J.; Collins, S. *Macromolecules* **2000**, *33*, 1508–1510.
(8) (a) Caporaso, L.; Cavallo, L. *Macromolecules* **2008**, *41*, 3439–3445. (b) Tomasi, S.; Weiss, H.; Ziegler, T. *Organometallics* **2007**, *26*, 2157–2166. (c) Caporaso, L.; Gracia-Budrìa, J.; Cavallo, L. *J. Am. Chem. Soc.* **2006**, *128*, 16649–16654. (d) Tomasi, S.; Weiss, H.; Ziegler, T. *Organometallics* **2006**, *25*, 3619–3630. (e) Hölscher, M.; Keul, H.; Höcker, H. *Macromolecules* **2002**, *35*, 8194–8202. (f) Hölscher, M.; Keul, H.; Höcker, H. *Chem.—Eur. J.* **2001**, *7*, 5419–5426. (g) Sustmann, R.; Sicking, W.; Bandermann, F.; Ferenz, M. *Macromolecules* **1999**, *32*, 4204–4213.
(9) (a) Cameron, P. A.; Gibson, V.; Graham, A. J. *Macromolecules* **2000**, *33*, 4329–4335. (b) Deng, H.; Shiono, T.; Soga, K. *Macromolecules* **1995**, *28*, 3067–3073. (c) Collins, S.; Ward, D. G.; Suddaby, K. H. *Macromolecules* **1994**, *27*, 7222–7224.
(10) (a) Miyake, G. M.; Caporaso, L.; Cavallo, L.; Chen, E. Y.-X. *Macromolecules* **2009**, *42*, 1462–1471. (b) Miyake, G. M.; Chen, E. Y.-X. *Macromolecules* **2008**, *41*, 3405–3416. (c) Miyake, G. M.; Mariott, W. R.; Chen, E. Y.-X. *J. Am. Chem. Soc.* **2007**, *129*, 6724–6725. (d) Mariott, W. R.; Chen, E. Y.-X. *Macromolecules* **2005**, *38*, 6822–6832. (e) Mariott, W. R.; Chen, E. Y.-X. *Macromolecules* **2004**, *37*, 4741–4743.
(11) (a) Bolig, A. D.; Chen, E. Y.-X. *J. Am. Chem. Soc.* **2001**, *123*, 7943–7944. (b) Chen, E. Y.-X.; Metz, M. V.; Li, L.; Stern, C. L.; Marks, T. J. *J. Am. Chem. Soc.* **1998**, *120*, 6287–6305. (c) Soga, K.; Deng, H.; Yano, T.; Shiono, T. *Macromolecules* **1994**, *27*, 7938–7940.
(12) (a) Razavi, A.; Thewalt, U. *J. Organomet. Chem.* **1993**, *445*, 111–114. (b) Razavi, A.; Ferrara, J. *J. Organomet. Chem.* **1992**, *435*, 299–310. (c) Ewen, J. A.; Jones, R. L.; Razavi, A.; Ferrara, J. D. *J. Am. Chem. Soc.* **1988**, *110*, 6255–6256.
(13) Rodriguez-Delgado, A.; Mariott, W. R.; Chen, E. Y.-X. *J. Organomet. Chem.* **2006**, *691*, 3490–3497.
(14) Kirillov, E.; Lehmann, C. W.; Razavi, A.; Carpentier, J.-F. *Organometallics* **2004**, *23*, 2768–2777.
(15) Qian, C.; Nie, W.; Chen, Y.; Sun, J. *J. Organomet. Chem.* **2002**, *645*, 82–86.

Scheme 2. Stereoerror Formation in MMA Polymerization by C_s-Ligated Catalysts

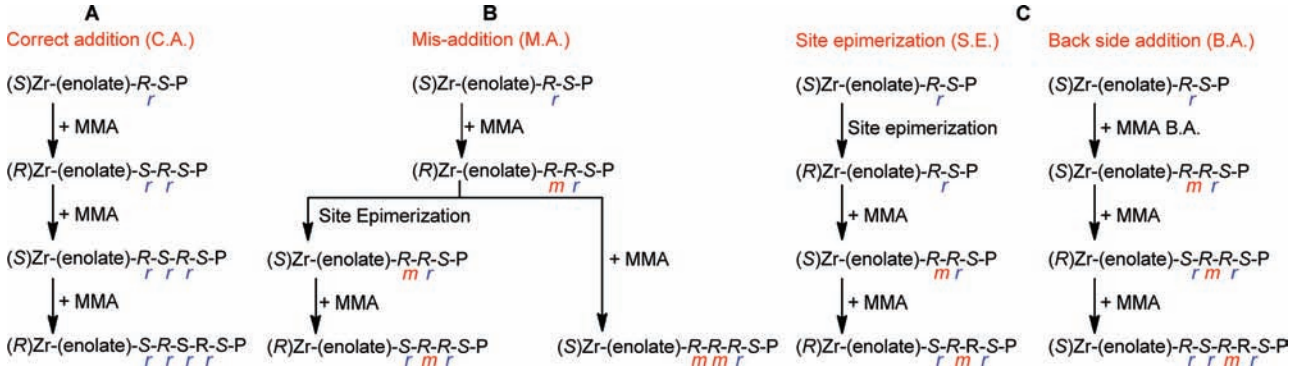

$[Me_2Si(Me_4Cp)(Flu)]YN(SiMe_3)_2$;[16] and $Me_2Si<$ bridged dysproso- and erbocenes, $[Me_2Si(Cp)(Flu)]LnE(SiMe_3)_2$ (Ln = Dy, Er; E = CH, N).[17] Like the C_s-ligated *ansa*-group 4 metallocene catalysts mentioned above, these C_s-ligated *ansa*-lanthanocene catalysts are even less active and syndioselective (~60% *rr* at 20 °C or ~82% *rr* at −95 °C) than the unbridged, C_{2v}-ligated $Cp^*_2LnR(THF)$-type catalysts. In addition, their catalyzed MMA polymerizations are also uncontrolled and give very low initiator efficiencies (I^* = 3−14%). Furthermore, methyl triad distributions of the PMMA prepared by these C_s-ligated *ansa*-lanthanocenes are characteristic of chain-end control. The $Me_2Si<$ bridged yttrocene, $[Me_2Si(Me_4Cp)(Flu)]YN(SiMe_3)_2$, even produced iso-rich PMMA (58% *mm* at 25 °C, 56% *mm* at 0 °C) in toluene, despite its C_s ligation.

The above-cited large number of C_s-ligated group 3 and 4 metallocene complexes that failed to lead to *st*-PMMA with appreciable syndiotacticity in a catalyst-site-controlled mechanism highlights the significant challenge in this effort and the complexity of C_s-ligated catalysts in coordination polymerization. In propylene polymerization by C_s-ligated catalysts, several pathways can introduce stereoerrors, including enantiofacial misinsertion (*mm* type), site epimerization (*m* type), "back-side" misinsertion (*mr* type), and chain epimerization (*m* or *mm* type).[18] In MMA polymerization by C_s-ligated catalysts, several possible pathways could, in principle, lead to *mm*- and *m*-type stereoerrors (Scheme 2). Starting with a chain where an *S*-catalyst selects a *si*-enolate chain end, this correct addition (C.A.) of MMA leads to an *S* chiral center in the chain and an *R* catalyst site; this regular migratory addition sequence then forms the syndiotactic polymer (*rrrr*..), case **A**. A misaddition (M.A.) affords a kinetic product (the higher energy RS than the RS after a correct addition); this stereomistake can be corrected either by catalyst-site epimerization to the thermodynamic RS followed by C.A. of MMA producing the isolated *m* dyad stereoerror, or by subsequent C.A. of MMA generating the *mm* type stereoerror (i.e., the enantiofacial misaddition error by a site-control mechanism), case **B**. Alternatively, the *m*-type stereoerror can also be generated either by the conventional site epimerization (S.E.) route typically seen in the propylene polymerization, or by back-side addition (B.A.) route, case **C**.

A rather successful example of MMA polymerization by the C_s-ligated catalyst, in terms of activity and polymerization control, involves the use of a CGC-type catalyst such as $\{(CGC)Ti(THF)[OC(O^iPr){=}CMe_2]\}^+[MeB(C_6F_5)_3]^-$ [CGC = $Me_2Si(\eta^5\text{-}(Me_4C_5)(^t BuN)$];[7c] however, it produces *st*-PMMA with modest syndiotacticity (80% *rr*, 18% *mr*, 2.0% *mm*) at room temperature with predominately isolated *m* meso dyad stereoerrors (...*rrrrmrrrr*...), pointing to the apparent chain-end control nature of this C_s-ligated catalysts.[7c] A combined experimental and theoretical study shows the monomer addition to be stereoselective and controlled by the chiral catalyst, while MMA- or counterion-assisted catalyst-site epimerization after a stereomistake, the process of which converts the kinetic product after a stereomistake into a thermodynamically more stable resting chelating intermediate, accounts for the formation of the predominately isolated *m* stereoerrors (Scheme 2).[7a] It is fascinating to point out here that, in the syndiospecific polymerization of propylene by C_s-ligated complexes, catalyst-site epimerization *generates m* stereoerrors, whereas in the polymerization of MMA by C_s-ligated complexes, catalyst-site epimerization *corrects* a stereomistake made in a previous enantiofacial misaddition (Scheme 2).

In light of the above unsuccessful attempts toward the site-controlled synthesis of highly syndiotactic PMMA, naturally it came as a big surprise when we first discovered, in 2008, that $Ph_2C<$ bridged, C_s-ligated *ansa*-zirconocene mono(ester enolate) and bis(ester enolate) complexes—which, upon activation with $B(C_6F_5)_3$ (as a THF adduct) and $[Ph_3C][B(C_6F_5)_4]$, generate the corresponding chiral cationic catalysts **3** and **4**, respectively (Chart 1)—produce highly syndiotactic PMMA (94% *rr*) at 25 °C via a predominately site-controlled mechanism.[19] Impressively, this high level of syndiotacticity remains even at a temperature of polymerization (T_p) of 50 °C (93% *rr*). This exciting discovery brought forth the following four important fundamental questions: (1) Why does this class of the $Ph_2C<$ bridged C_s-symmetric catalysts produce highly syndiotactic PMMA while others do not? (2) What is the role of the bridging atom and its substituents (i.e., $R_2E<$, R = Me vs Ph; E = C vs Si)? (3) How do ligand substitution, metal, anion, concentration, solvent, and temperature affect the polymerization characteristics, especially stereoregulation? (4) What are the general guidelines for devising a C_s-ligated catalyst with high activity and syndiospecificity based on what we have learned so far? Accordingly, the central objective of this study was to address these important questions both through experiments involving systematic variations of the catalyst or precatalyst structure

(16) Lee, M. H.; Hwang, J.-W.; Kim, Y.; Kim, J.; Han, Y.; Do, Y. *Organometallics* **1999**, *18*, 5124–5129.
(17) (a) Nie, W.; Qian, C.; Chen, Y.; Sun, J. *J. Organomet. Chem.* **2002**, *647*, 114–122. (b) Qian, C.; Nie, W.; Sun, J. *Organometallics* **2000**, *19*, 4134–4140.
(18) Chen, M.-C.; Roberts, J. A. S.; Marks, T. J. *J. Am. Chem. Soc.* **2004**, *126*, 4605–4625.
(19) Ning, Y.; Chen, E. Y.-X. *J. Am. Chem. Soc.* **2008**, *130*, 2463–2465.

Chart 1. *Ansa*-Zirconocene Complexes Incorporating C_s-Symmetric [R_2E(Cp)(Flu)]-Based Ligands and Their Variants Investigated in This Study

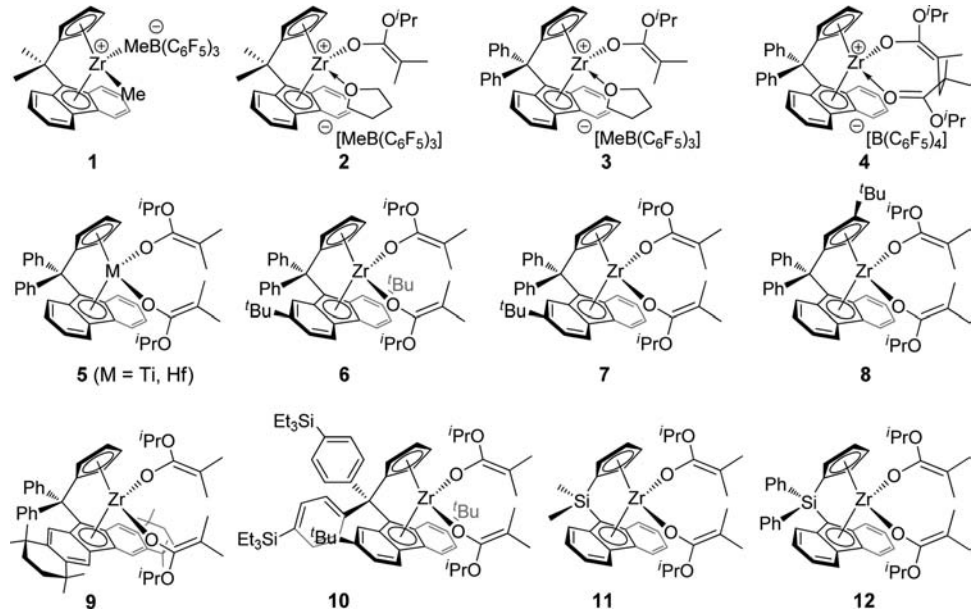

(Chart 1), activation methodology, and reaction conditions and through theoretical/computational investigations.

Experimental Section

[Ph_2C(Cp)(Flu)]Ti[OC(O^{i}Pr)=CMe_2]$_2$ (5, M = Ti). Anal. Calcd for $C_{45}H_{48}O_4Ti$: C, 77.13; H, 6.90. Found: C, 76.94; H, 6.71. ^{1}H NMR (C_7D_8, 23 °C): δ 8.02 (d, J = 7.8 Hz, 4H, Flu, Ph), 7.13 (t, J = 7.2 Hz, 4H, Flu), 6.88−6.81 (m, 8H, Ph), 6.35 (q, J = 2.7 Hz, 2H, Cp), 6.30 (d, J = 8.1 Hz, 2H, Flu), 6.28 (q, J = 2.7 Hz, 2H, Cp), 3.64 (sept, J = 6.3 Hz, 2H, C*H*Me$_2$), 1.51 (s, 6H, =C*Me*$_2$), 1.32 (s, 6H, =C*Me*$_2$), 0.98 (d, J = 6.0 Hz, 6H, CH*Me*$_2$), 0.88 (d, J = 6.3 Hz, 6H, CH*Me*$_2$). ^{13}C NMR (C_7D_8, 23 °C): δ 160.1 [O*C*(O^{i}Pr)=], 146.3, 138.2, 135.2, 131.7, 127.5, 126.9, 125.8, 125.3, 123.5, 121.3, 119.8, 115.2, 110.6, 74.27 (Flu, Ph, and Cp carbons), 89.80 (=*C*Me), 69.93 (*C*HMe$_2$), 58.71 (*C*Ph$_2$), 22.49, 22.11 (CH*Me*$_2$), 18.16, 17.92 (=C*Me*).

[Ph_2C(Cp)(Flu)]Hf[OC(O^{i}Pr)=CMe_2]$_2$ (5, M = Hf). Anal. Calcd for $C_{45}H_{48}O_4Hf$: C, 65.01; H, 5.82. Found: C, 64.74; H, 5.78. ^{1}H NMR (C_7D_8, 23 °C): δ 8.05 (d, J = 8.1 Hz, 2H, Flu), 7.84 (d, J = 8.1 Hz, 2H, Ph), 7.55 (d, J = 8.1 Hz, 2H, Ph), 7.15−6.78 (m, 12H, Flu, Ph), 6.32 (t, J = 2.6 Hz, 2H, Cp), 6.06 (t, J = 2.6 Hz, 2H, Cp), 3.64 (sept, J = 6.0 Hz, 2H, C*H*Me$_2$), 1.63 (s, 6H, =C*Me*$_2$), 1.44 (s, 6H, =C*Me*$_2$), 1.04 (d, J = 6.0 Hz, 6H, CH*Me*$_2$), 0.92 (d, J = 6.0 Hz, 6H, CH*Me*$_2$). ^{13}C NMR (C_7D_8, 23 °C): δ 154.1 [O*C*(O^{i}Pr)=], 147.0, 130.5, 129.4, 129.2, 127.5, 127.4, 123.7, 123.1, 123.0, 122.8, 122.4, 120.8, 114.7, 103.0, 86.12 (Flu, Ph, and Cp carbons), 87.30 (=*C*Me), 68.84 (*C*HMe$_2$), 59.35 (*C*Ph$_2$), 22.56, 22.01 (CH*Me*$_2$), 18.30, 18.19 (=C*Me*).

[Ph_2C(Cp)(2,7-^{t}Bu$_2$-Flu)]Zr[OC(O^{i}Pr)=CMe_2]$_2$ (6). Anal. Calcd for $C_{53}H_{64}O_4Zr$: C, 74.34; H, 7.53. Found: C, 75.05; H, 7.61. ^{1}H NMR (C_6D_6, 23 °C): δ 8.08 (d, J = 8.8 Hz, 2H, Flu), 7.95 (d, J = 8.0 Hz, 2H, Ph), 7.54 (d, J = 8.0 Hz, 2H, Ph), 7.33 (d, J = 8.4 Hz, 2H, Flu), 7.16 (t, J = 7.6 Hz, 2H, Ph), 7.06 (t, J = 7.6 Hz, 2H, Ph), 6.98 (t, J = 7.2 Hz, 2H, Ph), 6.74 (s, 2H, Flu), 6.49 (m, 2H, Cp), 6.25 (m, 2H, Cp), 3.93 (sept, J = 6.0 Hz, 2H, C*H*Me$_2$), 1.64 (s, 6H, =C*Me*$_2$), 1.51 (s, 6H, =C*Me*$_2$), 1.21 (s, 18H, ^{t}Bu), 1.10 (d, J = 6.8 Hz, 6H, CH*Me*$_2$), 1.08 (d, J = 6.0 Hz, 6H, CH*Me*$_2$). ^{13}C NMR (C_6D_6, 23 °C): δ 154.8 [O*C*(O^{i}Pr)=], 148.7, 146.4, 130.5, 128.8, 127.1, 126.7, 123.0, 122.4, 122.3, 121.6, 119.6, 118.5, 115.3, 103.8, 87.42 (Flu, Ph, and Cp carbons), 84.93 (=*C*Me$_2$), 69.30 (*C*HMe$_2$), 58.66 (*C*Ph$_2$), 35.22 (*C*(CH$_3$)$_3$), 31.11 (C(*C*H$_3$)$_3$), 22.55, 22.11 (CH*Me*$_2$), 19.16, 17.83 (=C*Me*).

{[Ph_2C(Cp)(2,7-^{t}Bu$_2$-Flu)]Zr(THF)[OC(O^{i}Pr)=CMe_2]}$^+$[MeB(C_6F_5)$_3$]$^-$ {6a$^+$[MeB(C_6F_5)$_3$]$^-$}. ^{1}H NMR (C_7D_8, 23 °C): δ 7.90 (d, J = 8.8 Hz, 1H, Flu), 7.85 (d, J = 8.8 Hz, 1H, Flu), 7.74 (d, J = 8.0 Hz, 1H, Ph), 7.68 (d, J = 8.0 Hz, 1H, Ph), 7.30−6.94 (m, 10H, Flu, Ph), 6.38 (br, s, 3H, Cp, Flu), 5.90 (s, 1H, Cp), 5.66 (s, 1H, Cp), 5.55 (s, 1H, Cp), 3.67 (sept, J = 6.0 Hz, 1H, C*H*Me$_2$), 3.05 (q, J = 6.4 Hz, 2H, α-CH$_2$, THF), 2.91 (q, J = 6.0 Hz, 2H, α-CH$_2$, THF), 1.38 (s, 3H, =C*Me*), 1.30−1.22 (m, 4H, β-CH$_2$, THF), 1.19 (s, 3H, =C*Me*), 0.98 (s, 9H, ^{t}Bu), 0.95 (s, 9H, ^{t}Bu), 0.93 (br, s, 3H, B-*Me*) (note the B-*Me* peak appeared at 0.49 ppm in CD_2Cl_2), 0.89−0.80 (m, 6H, CH*Me*$_2$). ^{19}F NMR (C_7D_8, 23 °C): δ −131.9 (d, J_{F-F} = 19.7 Hz, 6F, *o*-F), −164.4 (t, J_{F-F} = 20.9 Hz, 3F, *p*-F), −166.9 (t, J_{F-F} = 18.8 Hz, 6F, *m*-F). ^{13}C NMR (CD_2Cl_2, 23 °C): δ 154.9 [O*C*(O^{i}Pr)=], 152.6, 151.8, 144.2, 143.9, 129.7, 129.6, 129.5, 129.3, 128.5, 127.7, 126.7, 126.4, 125.6, 125.0, 124.6, 123.6, 123.5, 122.9, 121.9, 121.4, 120.0, 119.6, 118.7, 117.8, 117.2, 108.0, 104.0, 89.85 (Flu, Ph, and Cp carbons; broad resonances for the C_6F_5 groups due to C−F coupling omitted), 85.98 (=*C*Me), 78.34 (α-*C*H$_2$, THF), 72.39 (*C*HMe$_2$), 59.08 (*C*Ph$_2$), 35.46, 35.01 (*C*(CH$_3$)$_3$), 30.54, 30.48 (C(*C*H$_3$)$_3$), 25.88 (β-*C*H$_2$, THF), 22.21, 21.66 (CH*Me*$_2$), 18.71, 17.43 (=C*Me*), 11.64 (B-*Me*).

{[Ph_2C(Cp)(2,7-^{t}Bu$_2$-Flu)]Zr[OC(O^{i}Pr)=CMeCH$_2$C(Me$_2$)C(O^{i}Pr)=O]}$^+$ [HB(C_6F_5)$_3$]$^-$ {6b$^+$[HB(C_6F_5)$_3$]$^-$}. ^{1}H NMR (CD_2Cl_2, 23 °C): δ 8.26 (d, J = 8.8 Hz, 1H, Flu), 8.09 (d, J = 8.8 Hz, 1H, Flu), 8.02 (d, J = 8.0 Hz, 1H, Ph), 7.98 (d, J = 8.0 Hz, 1H, Ph), 7.93 (d, J = 7.6 Hz, 2H, Ph), 7.62−7.39 (m, 8H, Flu, Ph), 6.62 (s, 1H, Flu), 6.54 (s, 1H, Flu), 6.54−6.52 (m, 1H, Cp), 5.97 (q, J = 2.9 Hz, 1H, Cp), 5.92 (q, J = 2.8 Hz, 1H, Cp), 5.84 (q, J = 2.8 Hz, 1H, Cp), 4.26 (sept, J = 6.0 Hz, 1H, C*H*Me$_2$), 3.31 (sept, J = 6.2 Hz, 1H, C*H*Me$_2$), 2.44 (d, ^2J = 15.2 Hz, 1H, C*H*$_2$), 1.58 (d, ^2J = 14.8 Hz, 1H, C*H*$_2$), 1.44 (s, 3H, =C*Me*), 1.30 (s, 3H, C*Me*$_2$), 1.24 (d, J = 6.4 Hz, 3H, CH*Me*$_2$), 1.18 (s, 3H, C*Me*$_2$), 1.10 (d, J = 6.4 Hz, 3H, CH*Me*$_2$), 1.07 (s, 18H, ^{t}Bu), 1.04 (d, J = 6.4 Hz, 3H, CH*Me*$_2$), 0.94 (dd, ^1J = 6.0 Hz, 1H, B*H*), 0.84 (d, J = 6.0 Hz, 3H, CH*Me*$_2$). ^{19}F NMR (CD_2Cl_2, 23 °C): δ −132.2 (d, J_{F-F} = 22.3 Hz, 6F, *o*-F), −163.1 (t, J_{F-F} = 20.3 Hz, 3F, *p*-F), −165.9 (m, 6F, *m*-F). ^{13}C NMR (CD_2Cl_2, 23 °C): δ 190.7 [*C*(O^{i}Pr)=O], 155.80 [O*C*(O^{i}Pr)=], 153.5, 153.2, 144.0, 143.9, 129.7, 129.64, 129.59, 129.4, 128.0, 126.8, 126.7, 125.6, 124.2, 124.0, 123.7, 122.7, 121.8, 121.4, 120.7, 119.0, 117.6, 117.2, 115.2, 106.0, 102.8, 82.24 (Flu, Ph, C_6F_5, and Cp carbons; broad resonances for the C_6F_5 groups due to C−F coupling omitted), 86.52 (=*C*Me), 75.51, 68.87 (*C*HMe$_2$), 59.25

(*C*Ph$_2$), 47.59 (*C*Me$_2$), 40.58 (*C*H$_2$), 35.59, 35.43 (*C*(CH$_3$)$_3$), 31.93 (*C*Me$_2$), 30.82, 30.75 (C(*C*H$_3$)$_3$), 24.76 (*C*Me$_2$), 22.46, 22.10, 21.82, 21.33 (CH*Me*$_2$), 16.92 (=C*Me*). ^{11}B NMR (CD$_2$Cl$_2$, 23 °C): δ −25.4 (d, $^1J_{B-H}$ = 93.7 Hz).

{[Ph$_2$C(Cp)(2,7-^{t}Bu$_2$-Flu)] Zr[OC(O^{i}Pr)=CMe$_2$][O=C(O^{i}Pr)-CMe$_2$CH(CH=CH)$_2$C=CPh$_2$]}$^+$[B(C$_6$F$_5$)$_4$]$^-$ {6c$^+$[B(C$_6$F$_5$)$_4$]$^-$} and {[Ph$_2$C(Cp)(2,7-^{t}Bu$_2$-Flu)]Zr[OC(O^{i}Pr)=CMeCH$_2$C(Me$_2$)-C(O^{i}Pr)=O]}$^+$[B(C$_6$F$_5$)$_4$]$^-$ {6d$^+$[B(C$_6$F$_5$)$_4$]$^-$}. ^{1}H NMR (CD$_2$Cl$_2$, 300 MHz, −60 °C) for **6c**$^+$[B(C$_6$F$_5$)$_4$]$^-$: δ 6.60 (d, J = 11.7 Hz, 1H, Ph$_2$=C(C*H*=CH)$_2$CH), 6.58 (s, 2H, Flu), 6.55 (d, J = 12.6 Hz, 1H, Ph$_2$=C(C*H*=CH)$_2$CH), 6.32 (s, br, 1H, Cp), 6.00 (m, 1H, Cp), 5.84 (m, 1H, Cp), 5.79 (m, 1H, Cp), 5.58 (d, J = 9.6 Hz, 1H, C(CH=C*H*)$_2$CH), 5.02 (d, J = 9.6 Hz, 1H, C(CH=C*H*)$_2$CH), 4.80 (pent, J = 6.0 Hz, 1H, C*H*Me$_2$), 3.75 (pent, J = 6.0 Hz, 1H, C*H*Me$_2$), 3.37 (s, br, 1H, C(CH=CH)$_2$C*H*). ^{13}C NMR (CD$_2$Cl$_2$, 300 MHz, −60 °C) for **6c**$^+$[B(C$_6$F$_5$)$_4$]$^-$: δ 190.8 [*C*(O^{i}Pr)=O], 156.9 [O*C*(O^{i}Pr)=], 151.7, 151.1, 144.6, 143.8, 141.3, 131.0, 129.9, 129.8, 129.6, 128.7, 128.4, 128.1, 128.0, 127.1, 126.8, 126.5, 126.2, 125.4, 125.0, 124.8, 123.5, 123.1, 122.5, 121.5, 120.6, 119.0, 118.4, 117.7, 116.8, 107.1, 103.8, 84.73 (Flu, Ph, C$_6$F$_5$, and Cp carbons; broad resonances for the C$_6$F$_5$ groups due to C−F coupling omitted), 88.93 (=*C*Me$_2$), 76.96, 74.70 (O*C*HMe$_2$), 58.56 (*C*Ph$_2$), 49.22, 37.12 (*C*HMe$_2$), 35.92, 35.43 (*C*(CH$_3$)$_3$), 30.66, 30.50 (C(*C*H$_3$)$_3$), 22.31, 21.90, 21.29, 21.04 (CH*Me*$_2$), 18.39 (=C*Me*$_2$), 17.63 (CH*Me*$_2$). ^{1}H NMR (CD$_2$Cl$_2$, 300 MHz, −60 °C) for **6d**$^+$[B(C$_6$F$_5$)$_4$]$^-$ and Ph$_3$CH: δ 6.49 (s, 1H, Flu), 6.41 (s, 1H, Flu), 6.32 (s, br, 1H, Cp), 5.95 (m, 1H, Cp), 5.84 (m, 1H, Cp), 5.79 (m, 1H, Cp), 5.56 (s, 1H, Ph$_3$C*H*), 4.16 (pent, J = 6.2 Hz, 1H, C*H*Me$_2$), 3.20 (pent, J = 6.0 Hz, 1H, C*H*Me$_2$), 2.31 (d, ^2J = 14.8 Hz, 1H, C*H*$_2$), 1.50 (d, ^2J = 15.0 Hz, 1H, C*H*$_2$). ^{13}C NMR (CD$_2$Cl$_2$, 300 MHz, −60 °C) for **6d**$^+$[B(C$_6$F$_5$)$_4$]$^-$ and Ph$_3$CH: δ 190.3 [*C*(O^{i}Pr)=O], 156.2 [O*C*(O^{i}Pr)=], 154.0, 153.7 (Flu), 106.5, 103.2, 82.7 (Cp), 86.97 (=*C*Me), 75.95, 69.30 (O*C*HMe$_2$), 59.15 (*C*Ph$_2$), 57.46 (Ph$_3$*C*H), 48.03 (*C*Me$_2$), 41.00 (*C*H$_2$), 36.01, 35.86 (*C*(CH$_3$)$_3$), 32.33 (*C*Me$_2$), 31.03, 30.91 (C(*C*H$_3$)$_3$), 23.42 (*C*Me$_2$), 22.82, 22.49, 22.22, 21.96 (CH*Me*$_2$), 17.34 (=C*Me*). ^{19}F NMR (CD$_2$Cl$_2$, 282 MHz, −60 °C) for both **6c**$^+$[B(C$_6$F$_5$)$_4$]$^-$ and **6d**$^+$[B(C$_6$F$_5$)$_4$]$^-$: δ −131.7 (d, J = 12.7 Hz, 8F, *o*-F of C$_6$F$_5$), −161.0 (t, J = 21.0 Hz, 4F, *p*-F of C$_6$F$_5$), −164.9 (t, J = 18.9 Hz, 8F, *m*-F of C$_6$F$_5$).

{[Ph$_2$C(Cp)(2,7-^{t}Bu$_2$-Flu)]Zr[OC(O^{i}Pr)=CMe$_2$][O=C(O^{i}Pr)-CHMe$_2$]}$^+$[B(C$_6$F$_5$)$_4$]$^-$ {6e$^+$[B(C$_6$F$_5$)$_4$]$^-$} and {[Ph$_2$C(Cp)(2,7-^{t}Bu$_2$-Flu)]-Zr[OC(OMe)=CMeCH$_2$C(Me$_2$)C(O^{i}Pr)=O]}$^+$[B(C$_6$F$_5$)$_4$]$^-$ {6f$^+$[B(C$_6$F$_5$)$_4$]$^-$}. ^{1}H NMR (CD$_2$Cl$_2$, 300 MHz, −60 °C) for **6e**$^+$[B(C$_6$F$_5$)$_4$]$^-$: δ 8.14 (d, J = 8.7 Hz, 1H, Flu), 8.10 (d, J = 9.0 Hz, 1H, Flu), 7.97 (t, J = 6.2 Hz, 2H, Ph), 7.82−7.78 (m, 2H, Ph), 7.55−7.48 (m, 2H, Flu), 7.45−7.33 (m, 6H, Ph), 6.72 (q, J = 2.4 Hz, 1H, Cp), 6.42 (s, 1H, Flu), 6.39 (s, 1H, Flu), 6.03 (q, J = 2.4 Hz, 1H, Cp), 5.89−5.85 (m, 2H, Cp), 4.36 (sept, J = 6.0 Hz, 1H, C*H*Me$_2$), 3.63 (sept, J = 6.0 Hz, 1H, C*H*Me$_2$), 3.38 (q, J = 7.2 Hz, 8H, OC*H*$_2$CH$_3$), 2.07 (sept, J = 6.6 Hz, 1H, C*H*Me$_2$), 1.24 (s, 3H, =C*Me*$_2$), 1.19 (s, 3H, =C*Me*$_2$), 1.14−1.12 (d, br, 3H, CH*Me*$_2$), 1.11 (t, J = 7.2 Hz, 12H, OCH$_2$C*H*$_3$), 1.08−1.04 (t, J = 6.0 Hz, 6H, CH*Me*$_2$), 0.98 (s, 9H, ^{t}Bu), 0.97 (s, 9H, ^{t}Bu), 0.98−0.97 (m, 6H, CH*Me*$_2$), 0.92 (d, J = 6.9 Hz, 3H, CH*Me*$_2$). ^{19}F NMR (CD$_2$Cl$_2$, 282 MHz, −60 °C): δ −131.7 (d, J = 12.7 Hz, 8F, *o*-F of C$_6$F$_5$), −161.0 (t, J = 21.0 Hz, 4F, *p*-F of C$_6$F$_5$), −165.0 (t, J = 18.2 Hz, 8F, *m*-F of C$_6$F$_5$). ^{13}C NMR (CD$_2$Cl$_2$, −60 °C): δ 188.7 [*C*(O^{i}Pr)=O], 154.3 [O*C*(O^{i}Pr)=], 151.9, 150.8, 144.0, 143.6, 129.4, 129.3, 129.2, 129.0, 127.7, 126.5, 126.3, 124.7, 123.6, 122.9, 122.6, 122.2, 120.3, 119.2, 118.9, 118.0, 116.8, 116.7, 116.1, 105.6, 103.2, 84.62 (Flu, Ph, C$_6$F$_5$, and Cp carbons; broad resonances for the C$_6$F$_5$ groups due to C−F coupling omitted), 89.25 (=*C*Me$_2$), 75.56, 73.10 (O*C*HMe$_2$), 65.98 (O*C*H$_2$CH$_3$), 58.11 (*C*Ph$_2$), 36.75, 36.52 (*C*(CH$_3$)$_3$), 35.14 (*C*HMe$_2$), 30.40, 30.14 (C(*C*H$_3$)$_3$), 22.23, 22.02, 21.13, 21.05 (CH*Me*$_2$), 19.40, 18.72 (=C*Me*$_2$), 16.84 (CH*Me*$_2$), 15.28 (OCH$_2$*C*H$_3$).

^{1}H NMR (CD$_2$Cl$_2$, 300 MHz, −80 °C) for **6e**$^+$[B(C$_6$F$_5$)$_4$]$^-$ and MMA: δ 8.14 (d, J = 8.7 Hz, 1H, Flu), 8.09 (d, J = 8.7 Hz, 1H, Flu), 7.96 (d, J = 7.5 Hz, 2H, Ph), 7.78 (s, br, 2H, Ph), 7.50 (s, br, 2H, Flu), 7.44−7.32 (m, 6H, Ph), 6.73 (s, br, 1H, Cp), 6.36 (s, 1H, Flu), 6.35 (s, 1H, Flu), 6.03 (s, 2H, =C*H*$_2$, MMA, Cp), 5.87 (s, br, 2H, Cp), 5.57 (s, 1H, =C*H*$_2$, MMA), 4.31 (sept, J = 6.0 Hz, 1H, C*H*Me$_2$), 3.65 (s, 3H, O*Me*, MMA), 3.60 (sept, J = 6.0 Hz, 1H, C*H*Me$_2$), 3.36 (q, J = 7.0 Hz, 8H, OC*H*$_2$CH$_3$), 2.06 (sept, J = 6.3 Hz, 1H, C*H*Me$_2$), 1.85 (s, 3H, =C*Me*, MMA), 1.20 (s, 3H, =C*Me*$_2$), 1.16 (s, 3H, =C*Me*$_2$), 1.14−1.12 (d, br, 3H, CH*Me*$_2$), 1.09 (t, J = 7.0 Hz, 12H, OCH$_2$C*H*$_3$), 1.07−1.03 (t, J = 5.6 Hz, 6H, CH*Me*$_2$), 0.96 (s, 9H, ^{t}Bu), 0.94 (s, 9H, ^{t}Bu), 0.96−0.94 (m, 6H, CH*Me*$_2$), 0.89 (d, J = 6.9 Hz, 3H, CH*Me*$_2$). ^{19}F NMR (CD$_2$Cl$_2$, 282 MHz, −80 °C): δ −131.8 (d, J = 12.7 Hz, 8F, *o*-F of C$_6$F$_5$), −160.7 (t, J = 21.7 Hz, 4F, *p*-F of C$_6$F$_5$), −164.7 (t, J = 18.9 Hz, 8F, *m*-F of C$_6$F$_5$). ^{1}H NMR (CD$_2$Cl$_2$, 300 MHz, 20 °C) for **6f**$^+$[B(C$_6$F$_5$)$_4$]$^-$ and PMMA (only major peaks are reported here): δ 4.53 (sept, J = 6.0 Hz, 1H, C*H*Me$_2$), 4.26 (pent, J = 6.3 Hz, 1H, C*H*Me$_2$), 3.61 (s, br, O*Me*, PMMA), 2.93 (s, 3H, O*Me*), 2.42 (d, J = 15 Hz, 1H, C*H*$_2$), 2.24 (pent, J = 6.9 Hz, 1H, C*H*Me$_2$), 1.90 (s, br, C*H*$_2$, PMMA), 1.59 (d, J = 15 Hz, 1H, C*H*$_2$). ^{19}F NMR (CD$_2$Cl$_2$, 282 MHz, 20 °C): δ −131.4 (s, br, 8F, *o*-F of C$_6$F$_5$), −161.9 (t, J = 20.3 Hz, 4F, *p*-F of C$_6$F$_5$), −165.8 (t, J = 18.2 Hz, 8F, *m*-F of C$_6$F$_5$).

[Ph$_2$C(Cp)(2-^{t}Bu-Flu)]Zr[OC(O^{i}Pr)=CMe$_2$]$_2$ (7). Anal. Calcd for C$_{49}$H$_{56}$O$_4$Zr: C, 73.55; H, 7.05. Found: C, 73.28; H, 7.04. Selected crystal structural data for complex **7**: C$_{55}$H$_{56}$O$_4$Zr, T = 100(2) K, λ = 0.71073 Å, monoclinic, space group $P2_1/c$, a = 9.5340(9) Å, b = 11.8513(12) Å, c = 41.303(4) Å, β = 93.213(2)°, V = 4659.5(8) Å^3, Z = 4, D_{calcd} = 1.243 Mg/m^3, GOF on F^2 = 0.986, R_1 = 0.0555 and wR_2 = 0.1279 with $I > 2\sigma(I)$. ^{1}H NMR (C$_6$D$_6$, 23 °C): δ 8.10 (d, J = 8.4 Hz, 1H, Flu), 8.09 (d, J = 8.7 Hz, 1H, Flu), 7.93 (d, J = 8.1 Hz, 1H, Ph), 7.87 (d, J = 8.1 Hz, 1H, Ph), 7.69 (d, J = 8.1 Hz, 1H, Ph), 7.48 (d, J = 7.8 Hz, 1H, Ph), 7.30 (dd, ^3J = 8.7 Hz, ^4J = 1.5 Hz, 1H, Ph), 7.18−6.83 (m, 9H, Flu, Ph), 6.71 (d, ^4J = 1.5 Hz, 1H, Flu), 6.44 (q, J = 2.4 Hz, 1H, Cp), 6.33 (q, J = 2.4 Hz, 1H, Cp), 6.22 (q, J = 2.7 Hz, 1H, Cp), 6.15 (q, J = 2.7 Hz, 1H, Cp), 3.86 (sept, J = 6.2 Hz, 1H, C*H*Me$_2$), 3.76 (sept, J = 6.2 Hz, 1H, C*H*Me$_2$), 1.69 (s, 3H, =C*Me*$_2$), 1.62 (s, 3H, =C*Me*$_2$), 1.50 (s, 3H, =C*Me*$_2$), 1.48 (s, 3H, =C*Me*$_2$), 1.21 (s, 9H, ^{t}Bu), 1.07 (d, J = 6.3 Hz, 6H, CH*Me*$_2$), 1.04 (d, J = 6.3 Hz, 3H, CH*Me*$_2$), 0.96 (d, J = 6.3 Hz, 3H, CH*Me*$_2$). ^{13}C NMR (C$_6$D$_6$, 23 °C): δ 154.8 [O*C*(O^{i}Pr)=], 153.9 [*C*(O^{i}Pr)=O], 149.3, 146.4, 146.2, 130.4, 129.9, 128.80, 128.76, 128.6, 127.8, 127.1, 126.8, 126.7, 126.6, 126.5, 123.2, 122.8, 122.7, 122.5, 122.3, 121.3, 120.8, 119.9, 118.2, 115.5, 115.4, 104.3, 103.7, 86.67 (Flu, Ph, and Cp carbons), 85.91, 85.28 (=*C*Me), 69.35, 68.13 (*C*HMe$_2$), 58.78(*C*Ph$_2$), 35.18 (*C*(CH$_3$)$_3$), 31.02 (C(*C*H$_3$)$_3$), 22.54, 22.08, 21.99, 21.53 (CH*Me*$_2$), 18.90, 17.93, 17.86, 17.70 (=C*Me*).

[Ph$_2$C(3-^{t}Bu-Cp)(Flu)]Zr[OC(O^{i}Pr)=CMe$_2$]$_2$ (8). Anal. Calcd for C$_{49}$H$_{56}$O$_4$Zr: C, 73.55; H, 7.05. Found: C, 73.51; H, 6.82. ^{1}H NMR (C$_6$D$_6$, 23 °C): δ 8.12 (d, J = 8.0 Hz, 2H, Flu), 8.09 (d, J = 9.2 Hz, 1H, Ph), 7.96 (d, J = 8.0 Hz, 1H, Ph), 7.60 (d, J = 8.0 Hz, 1H, Ph), 7.55 (d, J = 8.0 Hz, 1H, Ph), 7.20−6.80 (m, 12H, Flu, Ph), 6.51 (t, J = 2.8 Hz, 1H, Cp), 6.28 (t, J = 3.0 Hz, 1H, Cp), 6.20 (t, J = 2.6 Hz, 1H, Cp), 3.73 (sept, J = 6.0 Hz, 2H, C*H*Me$_2$), 1.62 (s, 6H, =C*Me*$_2$), 1.50 (s, 3H, =C*Me*$_2$), 1.42 (s, 3H, =C*Me*$_2$), 1.22 (s, 9H, ^{t}Bu), 1.10 (d, J = 6.0 Hz, 3H, CH*Me*$_2$), 1.05 (d, J = 5.6 Hz, 3H, CH*Me*$_2$), 1.04 (d, J = 5.2 Hz, 3H, CH*Me*$_2$), 0.92 (d, J = 6.0 Hz, 3H, CH*Me*$_2$). ^{13}C NMR (C$_6$D$_6$, 23 °C): δ 155.0, 153.4 [O*C*(O^{i}Pr)=], 146.7, 146.3, 144.4, 130.3, 130.1, 128.8, 128.7, 128.6, 128.6, 127.8, 126.91, 126.86, 126.7, 126.3, 123.7, 123.10, 123.05, 122.83, 122.78, 122.6, 122.5, 122.3, 122.2, 122.1, 119.5, 112.6, 105.8, 102.1, 85.57 (Flu, Ph, and Cp carbons), 87.84, 87.19 (=*C*Me), 69.32, 68.47 (*C*HMe$_2$), 58.30 (*C*Ph$_2$), 32.70 (*C*(CH$_3$)$_3$), 31.00 (C(*C*H$_3$)$_3$), 22.32, 22.19, 21.42 (CH*Me*$_2$), 19.95, 18.95, 18.36, 18.22 (=C*Me*).

[Ph$_2$C(Cp)(Oct-Flu)]Zr[OC(O^{i}Pr)=CMe$_2$]$_2$ (9). Anal. Calcd for C$_{61}$H$_{76}$O$_4$Zr: C, 75.96; H, 7.94. Found: C, 75.95; H, 7.92. ^{1}H NMR (C$_6$D$_6$, 23 °C): δ 8.33 (s, 2H, Flu), 7.94 (d, J = 7.6 Hz, 2H, Ph), 7.50 (d, J = 8.0 Hz, 2H, Ph), 7.16 (t, J = 7.6 Hz, 2H, Ph), 7.09 (t, J = 7.6 Hz, 2H, Ph), 6.99 (t, J = 7.2 Hz, 2H, Ph), 6.75 (s, 2H, Flu), 6.38 (s, 2H, Cp), 6.13 (s, 2H, Cp), 3.87 (sept, J = 6.0 Hz,

2H, C*H*Me$_2$), 1.84 (m, 4H, CH_2), 1.67 (s, 6H, =CMe_2), 1.64−1.62 (m, 2H, CH_2), 1.56 (s, 6H, =CMe_2), 1.54−1.52 (m, 2H, CH_2), 1.42 (s, 6H, CH_3), 1.39 (s, 6H, CH_3), 1.16 (s, 6H, CH_3), 1.15 (s, 6H, CH_3), 1.08 (d, J = 6.0 Hz, 6H, CHMe_2), 1.05 (d, J = 6.0 Hz, 6H, CHMe_2). ^{13}C NMR (C_6D_6, 23 °C): δ 155.3 [O*C*(O^{i}Pr)=], 146.4, 144.9, 141.2, 130.7, 128.8, 128.7, 127.1, 126.6, 122.8, 122.0, 120.7, 120.3, 119.8, 115.6,103.7, 84.60 (Flu, Ph, and Cp carbons), 85.00 (=*C*Me), 68.24 (*C*HMe$_2$), 58.70 (*C*Ph$_2$), 35.64, 35.41, 35.21, 35.04 (*C*H$_0$ and *C*H$_2$), 33.53, 33.08, 32.37, 30.82 (*C*H$_3$), 22.60, 22.20 (CH*Me*$_2$), 19.20, 17.98 (=C*Me*).

[(p-Et$_3$SiPh)$_2$C(Cp)(2,7-^{t}Bu$_2$-Flu)]Zr[OC(O^{i}Pr)=CMe$_2$]$_2$ (10). Anal. Calcd for $C_{65}H_{92}O_4Si_2Zr$: C, 71.97; H, 8.55. Found: C, 71.71; H, 8.62. ^{1}H NMR (C_6D_6, 23 °C): δ 8.12 (dd, ^3J = 7.8 Hz, ^4J = 1.2 Hz, 2H, Ph), 8.10 (d, J = 8.8 Hz, 2H, Flu), 7.74 (dd, ^3J = 7.8 Hz, ^4J = 1.2 Hz, 2H, Ph), 7.50 (d, J = 8.0 Hz, 2H, Ph), 7.41 (d, J = 8.0 Hz, 2H, Ph), 7.34 (d, J = 8.4 Hz, 2H, Flu), 6.79 (s, 2H, Flu), 6.53 (t, J = 2.6 Hz, 2H, Cp), 6.33 (t, J = 2.6 Hz, 2H, Cp), 3.94 (sept, J = 6.2 Hz, 2H, C*H*Me$_2$), 1.64 (s, 6H, =CMe_2), 1.51 (s, 6H, =CMe_2), 1.23 (s, 18H, ^{t}Bu), 1.10 (d, J = 6.4 Hz, 6H, CHMe_2), 1.08 (d, J = 6.0 Hz, 6H, =CMe_2), 0.93 (t, J = 8.0 Hz, 18H, CH_3CH$_2$Si), 0.69 (q, J = 8.0 Hz, 12H, CH$_3$CH_2Si). ^{13}C NMR (C_6D_6, 23 °C): δ 155.2 [O*C*(O^{i}Pr)=], 149.1, 147.2, 136.2, 135.3, 135.2, 130.3, 126.9, 123.4, 122.8, 122.7, 121.9, 120.0, 118.9, 115.7, 104.3, 87.79 (Flu, Ph, and Cp carbons), 85.34 (=*C*Me), 69.73 (*C*HMe$_2$), 59.09 (*C*Ph$_2$), 35.65 (*C*(CH$_3$)$_3$), 31.61 (C(*C*H$_3$)$_3$), 22.92, 22.50 (CH*Me*$_2$), 19.59, 18.22 (=C*Me*), 8.00 (*C*H$_3$CH$_2$Si), 4.03 (CH$_3$*C*H$_2$Si).

[Me$_2$Si(Cp)(Flu)]Zr[OC(O^{i}Pr)=CMe$_2$]$_2$ (11). Selected crystal structural data for complex **11**: $C_{34}H_{44}O_4SiZr$, T = 120(2) K, λ = 0.71073 Å, triclinic, space group $P\bar{1}$, a = 10.8310(4) Å, b = 12.4790(4) Å, c = 14.1278(5) Å, α = 90.664(2)°, β = 111.403(2)°, γ = 113.539(2)°, V = 1601.96(10) Å^3, Z = 2, D_{calcd} = 1.319 Mg/m^3, GOF on F^2 = 1.030, R_1 = 0.0299 and wR_2 = 0.0737 with $I > 2\sigma(I)$. ^{1}H NMR (C_6D_6, 23 °C): δ 8.03 (d, J = 7.8 Hz, 2H, Flu), 7.55 (d, J = 7.8 Hz, 2H, Flu), 7.18−7.08 (m, 6H, Flu), 6.56 (t, J = 2.4 Hz, 2H, Cp), 6.02 (t, J = 2.4 Hz, 2H, Cp), 3.67 (sept, J = 6.2 Hz, 2H, C*H*Me$_2$), 1.57 (br, s, 12H, =CMe_2), 1.10 (d, J = 6.3 Hz, 6H, CHMe_2), 1.00 (d, J = 6.3 Hz, 6H, CHMe_2), 0.77 (s, 6H, SiMe_2). ^{13}C NMR (C_6D_6, 23 °C): δ 154.5 [O*C*(O^{i}Pr)=], 133.1, 130.1, 127.0, 123.5, 122.9, 122.5, 120.6, 113.6, 110.7 (Flu and Cp carbons), 86.47 (=*C*Me), 68.35 (*C*HMe$_2$), 22.16, 21.72 (CH*Me*$_2$), 17.74 (=C*Me*), −1.18 (Si*Me*$_2$).

[Ph$_2$Si(Cp)(Flu)]Zr[OC(O^{i}Pr)=CMe$_2$]$_2$ (12). Anal. Calcd for $C_{44}H_{48}O_4SiZr$: C, 69.52; H, 6.36. Found: C, 69.44; H, 6.24. ^{1}H NMR (C_6D_6, 23 °C): δ 8.08−8.05 (m, 6H, Flu, Ph), 7.27−7.10 (m, 10H, Flu, Ph), 6.88 (t, J = 7.6 Hz, 2H, Flu), 6.71 (m, 2H, Cp), 6.41 (m, 2H, Cp), 3.58 (sept, J = 6.0 Hz, 2H, C*H*Me$_2$), 1.63 (br, s, 6H, =CMe_2), 1.44 (br, s, 6H, =CMe_2), 1.04 (d, J = 6.0 Hz, 6H, CHMe_2), 0.91 (d, J = 6.0 Hz, 6H, CHMe_2). ^{13}C NMR (C_6D_6, 23 °C): δ 155.0 [O*C*(O^{i}Pr)=], 135.4, 135.1, 132.9, 131.1, 130.5, 129.3, 127.6, 124.4, 124.0, 123.3, 121.6, 115.3, 107.2, 66.17 (Flu, Ph, and Cp carbons), 87.13 (=*C*Me), 68.84 (*C*HMe$_2$), 22.58, 22.00 (CH*Me*$_2$), 18.39, 18.10 (=C*Me*).

Results and Discussion

Synthesis of Precatalysts and Generation of Cationic Ester Enolate Catalysts. The synthesis of the herein-described bis(ester enolate) complexes, L$_2$Zr[OC(O^{i}Pr)=CMe$_2$]$_2$, was carried out in a straightforward fashion by the reaction of the corresponding dichloride precursors L$_2$ZrCl$_2$ and the isolated, structurally characterized Me$_2$C=C(O^{i}Pr)OLi.[7a,20] Two of the C_s-ligated zirconocene bis(ester enolate) complexes have been structurally characterized (see Figures 1 and 2). The central five-membered ring of the Flu moiety in both Ph$_2$C< bridged **7** and Me$_2$Si< bridged **11** is best described as being η^3-bonded to Zr because

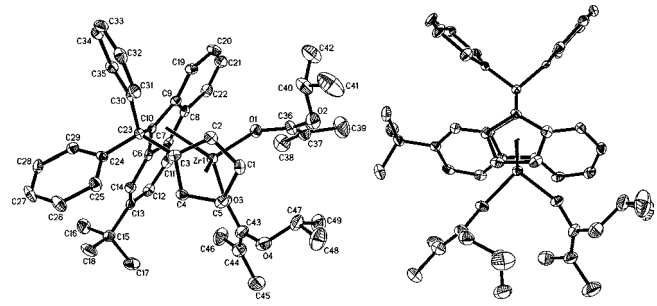

Figure 1. Molecular structure of [Ph$_2$C(Cp)(2-^{t}Bu-Flu)]Zr[OC(O^{i}Pr)=CMe$_2$]$_2$ (**7**) with thermal ellipsoids drawn at the 50% probability. Selected bond lengths (Å): Zr−O(1) = 1.964(3), Zr−O(3) = 1.981(3), Zr−C(1) = 2.546(4), Zr−C(2) = 2.491(4), Zr−C(3) = 2.490(4), Zr−C(4) = 2.486(4), Zr−C(5) = 2.539(4), Zr−C(6) = 2.575(4), Zr−C(9) = 2.571(4), Zr−C(10) = 2.491(4), Zr−C(7) = 2.735(4), Zr−C(8) = 2.727(4).

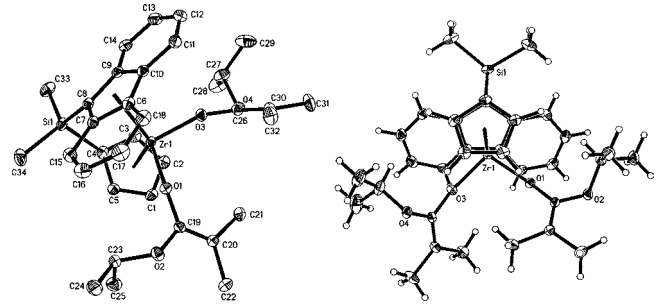

Figure 2. Molecular structure of [Me$_2$Si(Cp)(Flu)]Zr[OC(O^{i}Pr)=CMe$_2$]$_2$ (**11**) with thermal ellipsoids drawn at the 50% probability. Selected bond lengths (Å): Zr−O(1) = 1.9923(8), Zr−O(3) = 1.9698(7), Zr−C(1) = 2.5308(10), Zr−C(2) = 2.5416(11), Zr−C(3) = 2.4922(11), Zr−C(4) = 2.5007(10), Zr−C(5) = 2.4874(10), Zr−C(7) = 2.6173(10), Zr−C(8) = 2.4975(10), Zr−C(9) = 2.6117(10), Zr−C(6) = 2.7378(10), Zr−C(10) = 2.7611(10), Zr−Cp(centroid) = 2.201, Zr−Flu(centroid) = 2.345.

the bond distances from Zr to the two wedge carbons of the ring (C7 and C8 in **7**; C6 and C10 in **11**) are ≥2.73 Å for only weak interactions. The methyl mono(ester enolate) complexes, L$_2$ZrMe[OC(O^{i}Pr)=CMe$_2$], were synthesized using a three-step approach we developed earlier,[21] starting from L$_2$ZrMe$_2$ to L$_2$ZrMe(OTf) and last to L$_2$ZrMe[OC(O^{i}Pr)=CMe$_2$]$_2$.

The importance of employing cationic ester enolate complexes for MMA polymerization has been well-documented.[4,5] As such complexes bypass the slow initiation step involved in the polymerization by the typical alkyl complex and simulate the structure of true active propagating species, MMA polymerization by cationic ester enolate catalysts is typically much more active [by turnover frequency, TOF (h^{-1}) = moles of substrate (monomer) converted to product per mole of catalyst per hour], efficient (by initiator efficiency, I*), and controlled (by molecular weight, MW, and molecular weight distribution, MWD) than those mediated by the alkyl complexes. In this context, we focused on the best-performing catalyst derived from complex **6** (vide infra) and explored *four* different ways to generate the cationic ester enolate catalyst from the corresponding bis(ester enolate) or methyl mono(ester enolate) complex, including (a) methide abstraction of the Zr−Me bond, (b) vinylogous hydride abstraction of the Zr−enolate moiety, (c) electrophilic addition to the enolate moiety, and (d) protonolysis of the Zr−enolate bond (Scheme 3).

(20) Rodriguez-Delgado, A.; Chen, E. Y.-X. *J. Am. Chem. Soc.* **2005**, *127*, 961–974.

(21) Mariott, W. R.; Rodriguez-Delgado, A.; Chen, E. Y.-X. *Macromolecules* **2006**, *39*, 1318–1327.

Scheme 3. Different Activation Mechanisms To Generate Cationic Ester Enolate Catalysts

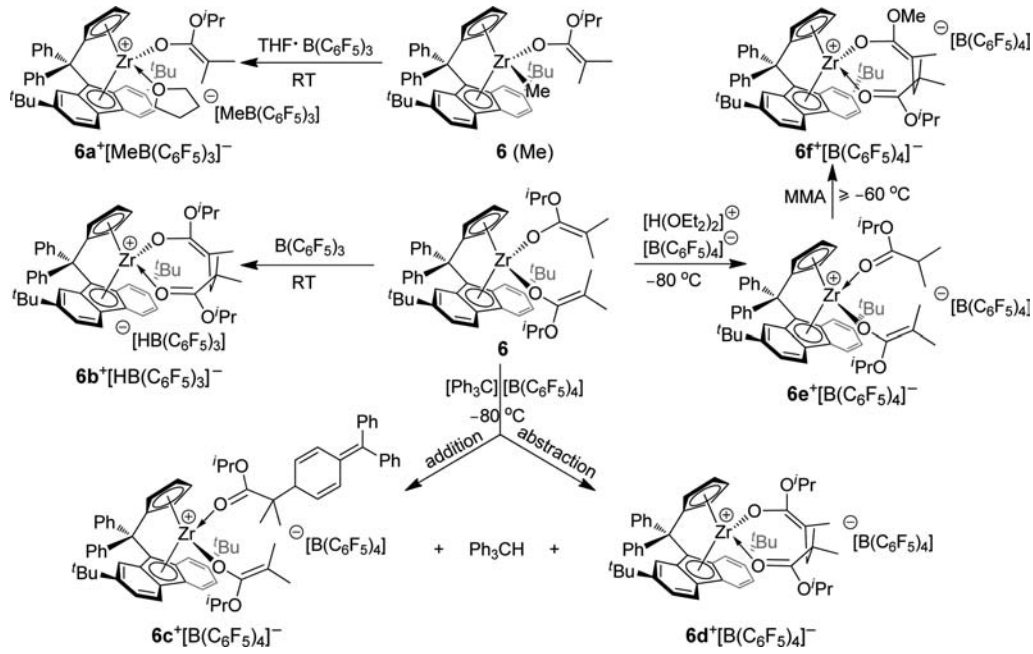

First, methide abstraction of the methyl mono(ester enolate) complex[4,19] by THF·$B(C_6F_5)_3$ at room temperature generates the corresponding cationic ester enolate complex **6a**$^+$[$MeB(C_6F_5)_3$]$^-$ (Scheme 3). The free [$MeB(C_6F_5)_3$]$^-$ anion is readily characterized by a broad singlet in ^{1}H NMR at 0.93 ppm (C_7D_8, 23 °C) or 0.49 ppm (CD_2Cl_2, 23 °C) for B−*Me*[22] and a small chemical shift difference of <3 ppm between the *para*- and *meta*-fluorines in ^{19}F NMR [Δ(*m*,*p*-F) = 2.5 ppm] for B−C_6F_5[23] in the non-coordinated methyl borate anion, while the ester enolate cation is characterized most notably by a septet at 3.67 ppm for the OC*H*Me_2 proton and ^{1}H NMR patterns and chemical shifts for the coordinated THF [3.05, 2.91 (q, 2H, α-CH_2), and 1.30−1.22 (m, 4H, β-CH_2)], as well as by a ^{13}C NMR chemical shift at 154.9 ppm (C_7D_8, 23 °C) for O*C*(O^iPr)═. Worthy of mention is its solubility in hydrocarbons such as toluene due to introduction of two *tert*-butyl groups to the Flu ring, in contrast to the parent, unsubstituted complex and many other THF-stabilized, separated metallocenium ion pairs which typically require the use of polar, chlorinated solvents to solubilize them.

Second, activation of the bis(ester enolate) complex by $B(C_6F_5)_3$ at room temperature affords cleanly the eight-membered-ring chelate ion pair **6b**$^+$[$HB(C_6F_5)_3$]$^-$ (Scheme 3). Without the readily abstractable methyl group on Zr, the strongly Lewis acidic borane undergoes vinylogous hydride abstraction from the Me group of the enolate [OC(O^iPr)═CMe_2] moiety to form [$HB(C_6F_5)_3$]$^-$ and the resulting isopropyl methacrylate coordinated to Zr; subsequent nucleophilic addition of the second enolate ligand on Zr to this coordinated isopropyl methacrylate (i.e., activated monomer) produces the cationic eight-membered-ring chelate **6b**$^+$[$HB(C_6F_5)_3$]$^-$. This ion pair exhibits spectroscopic signatures (see Figures 3 and 4) for (a) the uncoordinated [$HB(C_6F_5)_3$]$^-$ anion[24,25] [B*H* at 0.94 ppm (dd, ^1J = 6.0 Hz) in the ^{1}H NMR spectrum, a small chemical shift difference of 2.50 ppm between the *para*- and *meta*-fluorines in the ^{19}F NMR spectrum, and a *B*H doublet at −25.4 ppm ($^1J_{B-H}$ = 93.7 Hz) in the ^{11}B NMR spectrum] and (b) the cationic eight-membered-ring chelate[4,26] [most notably the two diastereotopic CH_2 protons at 2.44 (d) and 1.58 ppm (d) as well as coexistence of both the datively bound ester chain end (δ 4.26, sept. for OC*H*Me_2 in ^{1}H NMR and δ 190.7 for *C*(O^iPr)═O in ^{13}C NMR) and the covalently bound ester enolate (δ 3.31, sept. for OC*H*Me_2 and δ 155.8 for O*C*(O^iPr)═) entities].

Third, treatment of bis(ester enolate) complex **6** with [Ph_3C][$B(C_6F_5)_4$] at −80 °C in CD_2Cl_2 cleanly affords a mixture containing **6c**$^+$[$B(C_6F_5)_4$]$^-$, **6d**$^+$[$B(C_6F_5)_4$]$^-$, and Ph_3CH (δ 5.56, s, Ph_3CH) in a 4:1:1 ratio (Scheme 3). The eight-membered chelate **6d**$^+$[$B(C_6F_5)_4$]$^-$ is stable from −80 °C to room temperature, but complex **6c**$^+$[$B(C_6F_5)_4$]$^-$ is unstable at temperatures ≥ −30 °C, undergoing decomposition and release of additional Ph_3CH upon warming. The formation of **6c**$^+$[$B(C_6F_5)_4$]$^-$ is proposed to follow the same pathway as we previously elucidated for the reaction of silyl ketene acetal Me_2C═C(OMe)O$SiMe_3$ with 0.5 equiv of [Ph_3C][$B(C_6F_5)_4$] at −80 °C, which proceeds with *electrophilic addition* of Ph_3C^+, via the *para*-carbon of Ph, to the acetal to cleanly form the addition product [Ph_2C═C(CH═CH)$_2$C$HCMe_2$C(OMe)═O···$SiMe_3$][$B(C_6F_5)_4$].[27] Note that this adduct is identical to complex **6c**$^+$[$B(C_6F_5)_4$]$^-$, except for a different cation (Me_3Si^+ vs Zr^+). The formation of **6d**$^+$[$B(C_6F_5)_4$]$^-$ and Ph_3CH also parallels our previous finding that vinylogous hydride abstraction of the acetal by Ph_3C^+ at higher temperatures generates Me_3Si^+-activated MMA, which is attacked by the remaining acetal to form the corresponding Michael addition product [Me_3SiOC(OMe)═C$MeCH_2CMe_2$C(OMe)═O···$SiMe_3$][$B(C_6F_5)_4$] at −50 °C, with concomitant formation of Ph_3CH. Hydride abstraction from an enolate methyl group of

(22) Klosin, J.; Roof, G. R.; Chen, E. Y.-X.; Abboud, K. A. *Organometallics* **2000**, *19*, 4684–4686.
(23) Horton, A. D.; de With, J.; van der Linder, A. J.; van de Weg, H. *Organometallics* **1996**, *15*, 2672–2674.
(24) Garner, L. E.; Zhu, H.; Hlavinka, M. L.; Hagadorn, J. R.; Chen, E. Y.-X. *J. Am. Chem. Soc.* **2006**, *128*, 14822–14823.
(25) Yang, X.; Stern, C. L.; Marks, T. J. *Angew. Chem., Int. Ed.* **1992**, *31*, 1375–1377.
(26) Ning, Y.; Chen, E. Y.-X. *Macromolecules* **2006**, *39*, 7204–7215.
(27) Zhang, Y.; Chen, E. Y.-X. *Macromolecules* **2008**, *41*, 36–42.

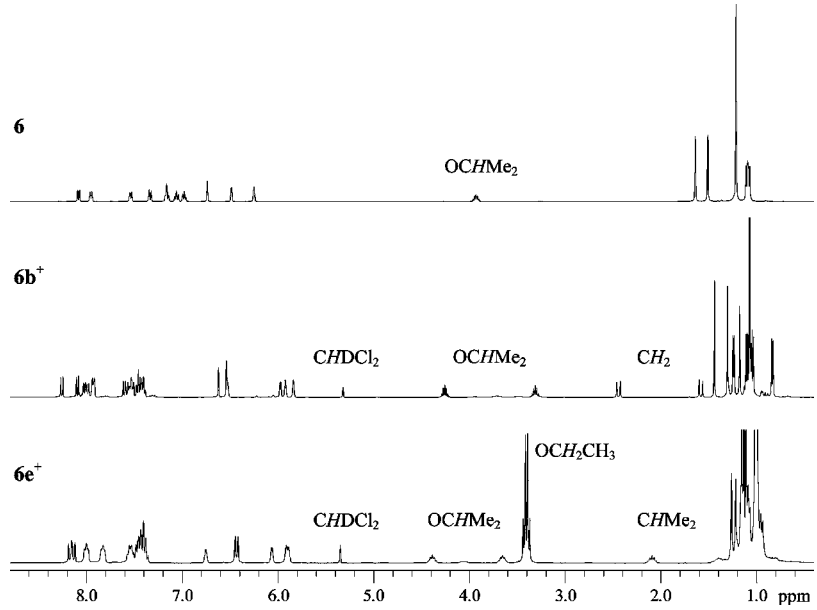

Figure 3. ^{1}H NMR spectra of precatalyst **6** (top, C_6D_6, 23 °C) as well as cationic ester enolate catalysts **6b**$^+$[HB(C_6F_5)$_3$]$^-$ (middle, CD_2Cl_2, 23 °C) and **6e**$^+$[B(C_6F_5)$_4$]$^-$ (bottom, CD_2Cl_2, −60 °C). Only the most diagnostic peaks are assigned here (see Experimental Section for complete assignments).

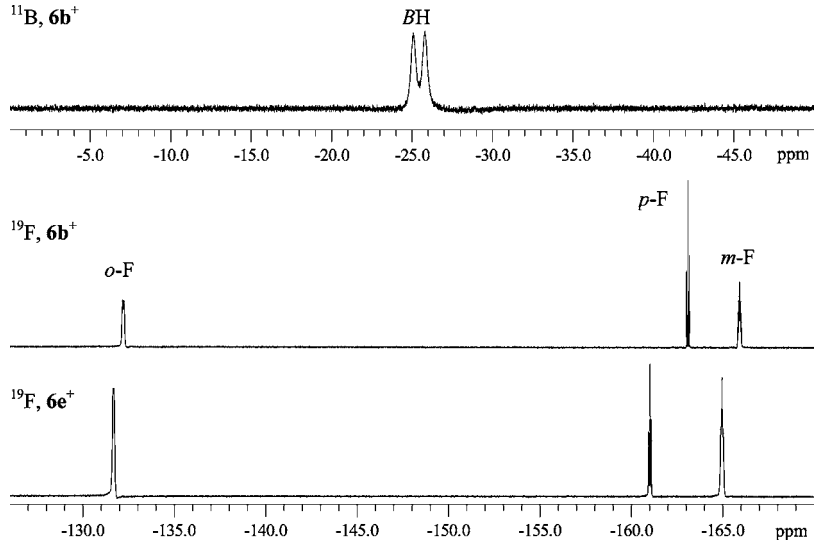

Figure 4. ^{11}B NMR (CD_2Cl_2) (top, 23 °C) and ^{19}F NMR (middle, 23 °C) spectra of **6b**$^+$[HB(C_6F_5)$_3$]$^-$ (top, 23 °C) and ^{19}F NMR (CD_2Cl_2) spectrum of **6e**$^+$[B(C_6F_5)$_4$]$^-$ (bottom, −60 °C).

$Cp_2ZrMe[OC(O^tBu)=CMe_2]$ by Ph_3C^+ was also reported to lead to the formation of a zirconium carboxylate dication after subsequent elimination of methane and isobutene.[5c]

Fourth, through protonolysis of the Zr−enolate bond with a strong acid,[7d] the reaction of bis(ester enolate) complex **6** with [H(Et_2O)$_2$][B(C_6F_5)$_4$] at −80 °C cleanly generates cationic ester enolate complex **6e**$^+$[B(C_6F_5)$_4$]$^-$ (Scheme 3), which is stabilized by isopropyl isobutyrate, the protonolysis coproduct, and is stable at −60 °C. Spectral changes correlate with the transformation of the C_s-symmetric neutral bis(ester enolate) **6** to the C_1-symmetric cationic ester enolate complex **6e**$^+$[B(C_6F_5)$_4$]$^-$, and the spectral features of the cation are characteristic of the isopropyl isobutyrate-stabilized cationic zirconocene ester enolate, including key chemical shifts in ^{1}H NMR (CD_2Cl_2, −60 °C) at δ 4.36 (sept, OC*H*Me$_2$, enolate), 3.63 (sept, OC*H*Me$_2$, isobutyrate), and 2.07 (sept, C*H*Me$_2$, isobutyrate) for the C*H*Me$_2$ group present in the covalently bound ester enolate ligand and the datively bound isobutyrate ligand, as well as in ^{13}C NMR at δ 188.7 and 154.3 for the ester *C*(O^{i}Pr)=O and enolate O*C*(O^{i}Pr)= carbons, respectively. Addition of MMA to this cationic solution at ≥ −60 °C led to the formation of the eight-membered chelate **6f**$^+$[B(C_6F_5)$_4$]$^-$ and subsequent PMMA formation. From this set of variable-temperature NMR experiments, we accomplished the detection and characterization of all key species involved in the catalyst formation and polymerization initiation and propagation—from the precatalyst to the cationic active species to the resting intermediate and finally to the polymer—thereby providing critical insight into the polymerization mechanism (vide infra).

Characteristics of Polymerization by Catalysts Derived from Complexes 3−12. The above understanding of how the ester enolate precatalysts are activated into active cationic species also gave us important perspectives as to what activators to use for polymerizations. Over the course of this study, we found that the catalyst systems derived from the activation using [Ph_3C][B(C_6F_5)$_4$] at ambient temperature using the in-reactor

Table 1. Results of MMA Polymerization by Catalysts Based on Complexes **3**−**12**[a]

run no.	catalyst	solvent	time (min)	conv[b] (%)	TOF (h^{-1})	M_n[c] ($\times 10^{-3}$ g/mol)	PDI[c] (M_w/M_n)	I^*[d] (%)	[*rr*][b] (%)	[*mr*][b] (%)	[*mm*][b](%)
1	**3**	DCM	15	50.0	800	41.5	1.48	48.6	94.2	4.0	1.8
2	**4**	DCM	15	44.8	717	44.3	1.32	41.1	93.5	4.5	2.0
3	**4**	TOL	15	30.6	490	28.5	1.56	43.9	93.7	4.3	2.0
4	**5**(Ti)	DCM	1440	0							
5	**5**(Hf)	DCM	1440	<0.5					92.9	4.6	2.4
6	**6**	TOL	15	97.1	1554	40.0	1.14	97.8	93.7	4.9	1.4
7	**7**	DCM	23	71.6	747	45.5	1.19	63.5	92.3	6.0	1.7
8	**8**	TOL	1440	0	0						
9	**9**	TOL	60	26.2	105	34.8	1.23	30.9	86.2	11.4	2.3
10	**10**	TOL	15	97.3	1557				94.0	4.2	1.8
11	**11**	TOL	1440	0	0						
12	**12**	TOL	1440	0	0						

[a] Carried out at ambient temperature (~25 °C) in 10 mL of toluene (TOL) or CH_2Cl_2 (DCM) + MMA solutions, where $[MMA]_0 = 0.935$ M and $[precatalyst]_0 = [activator]_0$ $\{[Ph_3C][B(C_6F_5)_4]\} = 2.34$ mM for a [MMA]/[catalyst] ratio of 400/1. [b] Monomer conversions and PMMA methyl triad distributions measured by ^{1}H NMR. [c] M_n and PDI determined by gel permeation chromatography relative to PMMA standards. [d] Initiator efficiency (I^*) = M_n(calcd)/M_n(exptl), where M_n(calcd) = MW(MMA) × $[MMA]_0/[catalyst]_0$ × conversion% + MW of chain-end groups.

activation methodology (see Experimental Section), which generates the corresponding ester enolate cation paired with the unassociated anion $[B(C_6F_5)_4]^-$, give the highest catalyst activity (TOF), polymerization efficiency (I^*), and polymer syndiotacticity (%*rr*). An exception here is the methyl mono(ester enolate) precatalyst, which is best activated cleanly with $THF \cdot B(C_6F_5)_3$ to the corresponding cationic catalyst (cf., complex **3**). Accordingly, in our study examining the relative TOF, I^*, %*rr*, and degree of polymerization control [number-average molecular weight (M_n) and polydispersity index (PDI)] of catalysts based on complexes **3**−**12**, we fixed the [MMA]/[catalyst] ratio to be 400/1 (and the MMA and catalyst concentrations) and the activator to be $[Ph_3C][B(C_6F_5)_4]$ (except for complex **3**); additionally all polymerizations were carried out at ambient temperature. The results of this comparative study are summarized in Table 1.

It can be seen from the table that, while the parent zirconocene catalysts **3** and **4** (no substitutions to either the Cp or Flu ring) produce *st*-PMMA with a remarkably high syndiotacticity at room temperature (94% *rr*),[19] they failed to achieve high monomer conversions (regardless of the reaction time), with low I^* of <50% and relatively broad MWD of >1.3 (runs 1−3). It should be mentioned that at a low [MMA]/[catalyst] ratio of 100/1, high quantitative monomer conversions can be achieved, and the resulting polymers exhibit narrower MWDs.[19] Furthermore, catalysts **3** polymerized 200 equiv of *n*-butyl methacrylate (BMA) in 1 h, achieving a 90% monomer conversion and producing *st*-PBMA with a high syndiotacticity of 94% *rr*; it also polymerized 200 equiv of DMAA in 30 min, achieving a 97% monomer conversion and producing highly syndiotactic PDMAA with T_m of 283 °C. On the other hand, their titanium and hafnium derivatives **5** exhibit either no activity (Ti, run 4)) or negligible activity (Hf, run 5) for MMA polymerization, although the Hf catalyst produced *st*-PMMA with a high syndiotacticity of 93% *rr*.

The catalyst derived from the di-*tert*-butyl-substituted Flu complex **6** is most remarkable in *all* aspects of the polymerization (run 6): TOF up to 1554 h^{-1} (thus *highly active*), nearly quantitative I^* of 98% (thus *highly efficient*), syndiotacticity of 94% *rr* (thus *highly syndiospecific*), and predicted M_n of 4.00×10^{-4} and narrow MWD of 1.14 (thus *well-controlled*). This catalyst system is also robust, producing highly syndiotactic PMMA at higher temperatures (e.g., 93% *rr* at 50 °C). PBMA produced by this catalyst is also highly syndiotactic (94% *rr*). Furthermore, from a polymerization process point of view, this catalyst offers an additional advantage because the di-*tert*-butyl substitution on the Flu ring made its cationic species it soluble in hydrocarbon solvents so that the polymerization can be readily carried out in less toxic solvents such as toluene, instead of CH_2Cl_2.

Removing one of the two ^{t}Bu groups on the Flu ring produced a less active and less efficient catalyst system, **7**. Interestingly, despite its C_1-ligation due to the uneven substitution on the Flu ring, this catalyst still affords highly syndiotactic PMMA (92% *rr*) at room temperature (run 7). However, placing a ^{t}Bu group on the Cp ring resulted in an inactive catalyst system, **8** (run 8). Intriguingly, catalyst **9**, based on the sterically expanded Oct-Flu ligation that furnished one of the most syndiospecific propylene polymerization catalysts,[28] is not only much less active (105 h^{-1} TOF) but also considerably less syndioselective (86% *rr*, run 9) than the parent catalyst **3** or **4**; its comparison with catalyst **6** is even more extreme.

By examining the electronic effect of the bridging aryl groups we found that catalyst **10**, with the Et_3Si group substituted on the *para*-Ph ring, performs nearly identically to catalyst **6** in terms of both polymerization activity and polymer syndiotacticity (run 10 vs 6). As a matter of fact, the apparent rate constants (k_{app}) of the two catalysts, obtained from the slopes of the best-fit lines to the first-order kinetic plots of $\ln([MMA]_0/[MMA]_t)$ vs time (Figure 5), are identical: $k_{app} = 0.31$ min^{-1}. Finally, the $Me_2Si<$ and $Ph_2Si<$ bridged C_s-catalysts **11** and **12** are inactive for MMA polymerization under the current reaction conditions. While the catalyst resulting from the activation of **12** with $B(C_6F_5)_3$ exhibits marginal activity (TOF ~2 h^{-1}), the PMMA produced has a low syndiotacticity of 63% *rr*.

Kinetics and Mechanism of Polymerization by Catalyst $6^+[B(C_6F_5)_4]^-$. Having established catalyst $6^+[B(C_6F_5)_4]^-$, derived from activation of precatalyst **6** with $[Ph_3C][B(C_6F_5)_4]$ by the in-reactor activation method, as the best catalyst system in all aspects for the MMA polymerization, we subsequently examined the MMA polymerization by this catalyst in more detail, specifically concerning its degree of control and kinetics.

Table 2 summarizes the kinetic results of the MMA polymerization with two different [MMA]/[Zr] ratios at 25 °C in toluene: a low ratio of 200 and a high ratio of 1000. As can be seen from this table, the MMA polymerization with a $[MMA]_0/[Zr]_0$ ratio of 200 is rapid, achieving a quantitative monomer conversion in 10 min. The initiator efficiencies I^* were modest in the low monomer conversion regime (49−86%, most likely

(28) Miller, S. A.; Bercaw, J. E. *Organometallisc* **2004**, *23*, 1777–1789.

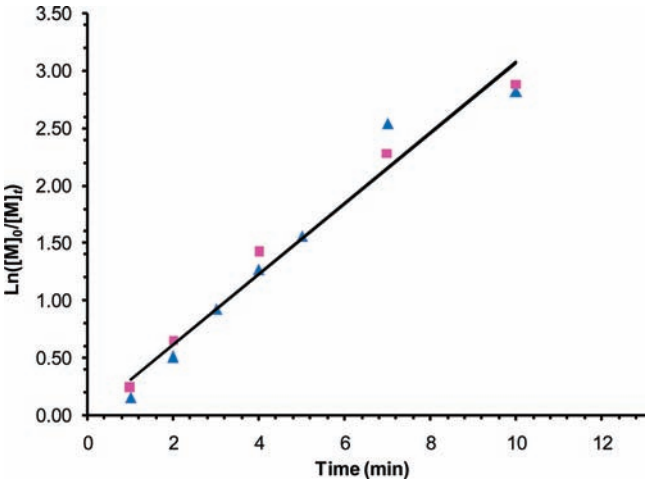

Figure 5. Plots of the first-order kinetics of $\ln([MMA]_0/[MMA]_t)$ vs time (min) for the polymerization of MMA by **6** (pink ■) and **10** (blue ▲) activated with equimolar $[Ph_3C][B(C_6F_5)_4]$ in toluene at 25 °C. Conditions: $[MMA]_0 = 0.935$ M, $[Zr]_0 = 2.34$ mM.

Table 2. Selected Results for MMA Polymerization by Catalyst $\mathbf{6}^+[B(C_6F_5)_4]^-$ in Toluene at 25 °C

run no.	time (min)	conv (%)	M_n ($\times 10^{-3}$ g/mol)	PDI (M_w/M_n)	I^* (%)
		[**6**] = 4.67 mmol/L, $[MAA]_0/[\mathbf{6}]_0 = 200$			
1	0.5	15.4	6.90	1.13	48.5
2	1.0	49.1	13.1	1.22	77.3
3	1.5	61.5	14.7	1.16	85.7
4	2.0	76.7	17.0	1.17	91.7
5	3.0	91.5	20.0	1.15	92.9
6	4.0	96.0	20.4	1.15	95.3
7	6.0	98.9	21.2	1.15	94.7
8	10	100	21.2	1.15	95.5
		[**6**] = 0.935 mmol/L, $[MAA]_0/[\mathbf{6}]_0 = 1000$			
9	1.5	15.1	16.0	1.15	96.2
10	3.0	33.6	29.3	1.16	115
11	5.0	51.1	40.2	1.17	128
12	7.0	63.6	47.1	1.19	136
13	10	71.7	53.3	1.18	135
14	15	79.8	58.9	1.20	136
15	25	88.8	66.8	1.20	134
16	40	93.9	67.1	1.25	141
17	120	98.9	70.0	1.26	142

due to errors associated with M_n measurements for low-MW polymer samples), but the I^* values were high (~95%) in the high monomer conversion regime with typical low PDI values ~1.15, consistent with a monometallic propagation mechanism (i.e., one polymer chain per metal center). This observation, together with the observed linear increase of M_n vs MMA conversion (with a nonzero intercept) while maintaining nearly constant low PDI values (Figure 6), demonstrates that the polymerization is well-controlled under the current conditions.

The polymerization with a high [MMA]/[Zr] ratio of 1000 is also controlled, as judged by a linear increase of M_n vs MMA conversion with low PDI values (Figure 7). However, the degree of control is less than the polymerization at lower [MMA]/[Zr] ratios, as evidenced by slowly increasing PDI and I^* values with increase in monomer conversion (Table 2, Figure 7). The I^* values of over 100% (128 −142%) with conversions >50% are indicative of chain-transfer reactions at later stages of the polymerization with this high [MMA]/[Zr] ratio of 1000. Nonetheless, the catalyst is not deactivated by such reactions, as the polymerization can proceed to nearly quantitative conversion in 2 h (run 17).

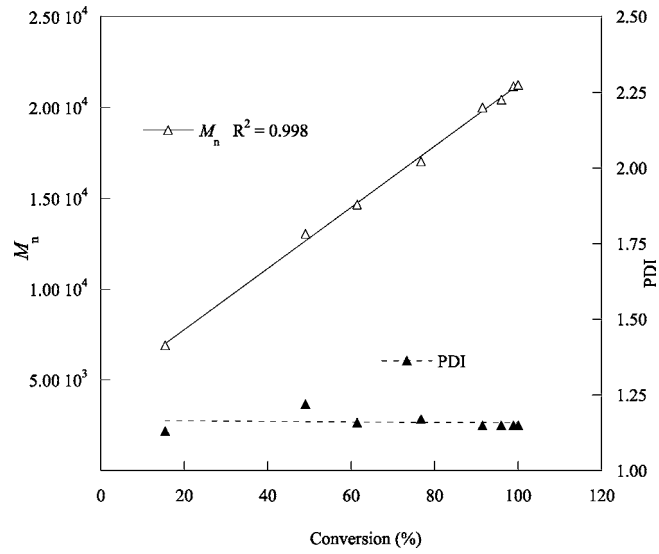

Figure 6. Plots of M_n and PDI of PMMA vs MMA conversion in toluene at 25 °C: $[MMA]_0 = 0.935$ M, $[\mathbf{6}]_0 = [Ph_3C][B(C_6F_5)_4]_0 = 4.67$ mM with a $[MMA]_0/[catalyst]_0$ ratio of 200/1.

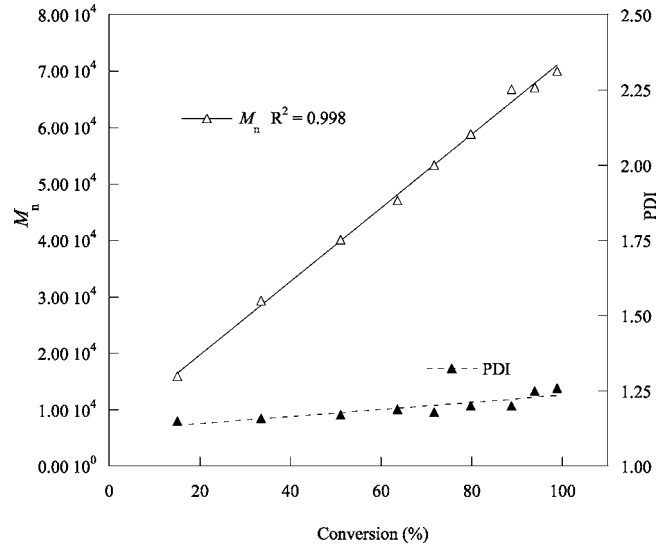

Figure 7. Plots of M_n and PDI of PMMA vs MMA conversion in toluene at 25 °C: $[MMA]_0 = 0.935$ M, $[\mathbf{6}]_0 = [Ph_3C][B(C_6F_5)_4]_0 = 0.935$ mM with a $[MMA]_0/[catalyst]_0$ ratio of 1000/1.

Kinetic experiments employed $[MMA]_0/[Zr]_0$ ratios ranging from 100 to 1000, clearly showing first-order dependence on [MMA] for all the ratios (Figure 8). Furthermore, a double logarithm plot (Figure 9) of the apparent rate constants (k_{app}), obtained from the slopes of the best-fit lines to the plots of $\ln([MMA]_0/[MMA]_t)$ vs time as a function of $\ln[Zr]_0$, was fit to a straight line ($R^2 = 0.99$) with a slope of 1.05. Thus, the kinetic order with respect to [Zr], given by the slope of 1, reveals that the propagation is also first-order in catalyst concentration, indicating that the MMA polymerization follows the monometallic, intramolecular coordination−addition mechanism, similar to that undergone by *ansa*-C_2-ligated catalysts.[4]

Overall, the above kinetic results, coupled with mechanistic insight obtained through monitoring the polymerization and identification of intermediates (vide supra), led to the proposed polymerization mechanism outlined in Scheme 4. Hence, the propagation "catalysis" cycle involves fast intramolecular Michael addition within catalyst−monomer complex **D**, leading

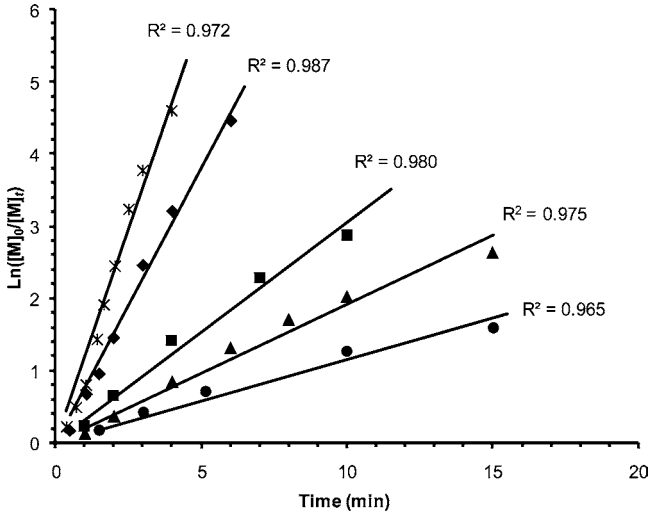

Figure 8. Plots of the first-order kinetics of $\ln([MMA]_0/[MMA]_t)$ vs time (min) for the polymerization of MMA by **6** activated with equimolar $[Ph_3C][B(C_6F_5)_4]$ in toluene at 25 °C. Conditions: $[MMA]_0 = 0.935$ M; $[Zr]_0 = 9.35$ (*), 4.67 (◆), 2.34 (■), 1.56 (▲), and 0.935 (●) mM.

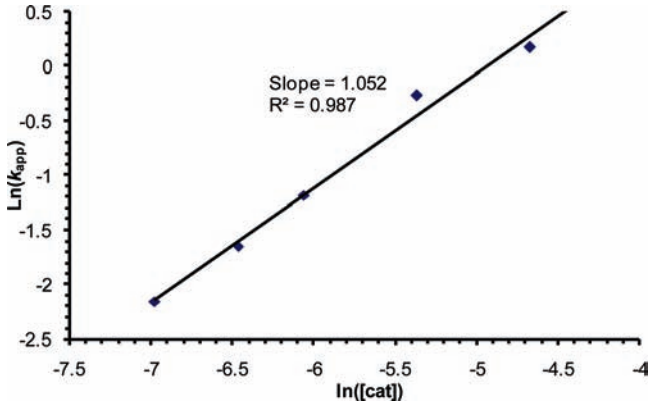

Figure 9. Plot of $\ln(k_{app})$ vs ln[Zr] for MMA polymerization by **6** in toluene at 25 °C.

Scheme 4. Proposed Mechanism of Methacrylate Polymerization Catalyzed by $\mathbf{6}^+[B(C_6F_5)_4]^-$

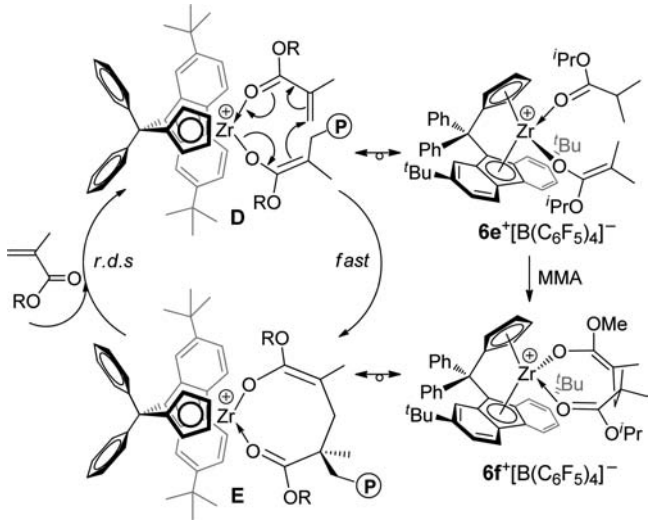

to the eight-membered cyclic ester enolate chelate (resting active intermediate **E**), followed by the slower, rate-limiting ring-opening of the chelate via frontside displacement of the coordinated ester group in **E** by the incoming monomer to regenerate **E** (by going through enantiomeric structures of **D** and **E**). In this scheme, catalyst−monomer complex **D** and catalyst resting intermediate **E** are simulated by complexes $\mathbf{6e}^+[B(C_6F_5)_4]^-$ and $\mathbf{6f}^+[B(C_6F_5)_4]^-$ (Schemes 3, 4, and Experimental Section), respectively.

Effects of Polymerization Conditions on Syndiospecificity. To understand the polymerization stereoregulation, we examined the effects of polymerization conditions on syndiospecificity of the MMA polymerization by catalyst $\mathbf{6}^+$. The polymerization conditions examined include monomer-to-catalyst ratio (concentration), temperature, solvent polarity, and activator (anion structure).

First, polymerization in toluene at 25 °C using catalyst $\mathbf{6}^+[B(C_6F_5)_4]^-$, derived from activation of precatalyst **6** with $[Ph_3C][B(C_6F_5)_4]$ by the in-reactor activation method, afforded *st*-PMMA with a constant syndiotacticity (93−94% *rr*) as the [MMA]/[catalyst] ratio was varied 20-fold from 100/1 to 2000/1 (runs 1−7, Table 3). However, close inspection of the methyl triad-level stereomicrostructure of PMMA revealed an important insight: at a low [MMA]/[catalyst] ratio of 100, a triad test of 2[*mm*]/[*mr*] gave 1.00 (run 1), characteristic of a perfect site-controlled mechanism, but at higher [MMA]/[catalyst] ratios (lower catalyst or higher monomer concentrations) the test deviated from unity, ranging from 0.77 to 0.52, due to either reduced enantiofacial misaddition errors (...*rrrrmmrrrr*...) or enhanced catalyst-site epimerization errors (...*rrrrmrrrr*...), or both (runs 2−7). This observation is intriguing because the trend for the isolated *m* meso dyad stereoerrors as a function of the [monomer]/[catalyst] ratio is opposite that observed for syndiospecific propylene polymerization by C_s-ligated catalysts.[29] This unique behavior in the MMA polymerization by C_s-ligated catalysts is further discussed in the next section.

Second, it is remarkable to see the syndiotacticity of PMMA remain constant (93−94% *rr*) as the polymerization temperature is varied from 0 (run 8) to 50 °C (run 9), showing the robustness of this catalyst system. However, the polymerization temperature does affect the T_m of the resulting *st*-PMMA: $T_m = 156.3$ °C for polymerization at 25 °C by $\mathbf{6}^+[B(C_6F_5)_4]^-$, and $T_m = 151.9$ and 163.5 °C for polymerizations by the parent catalyst $\mathbf{4}^+[B(C_6F_5)_4]^-$ at 50 and 0 °C, respectively (Figure 10).

Third, this polymerization is also insensitive to solvent polarity, again in marked contrast to the propylene polymerization. Thus, switching the solvent from toluene ($\varepsilon = 2.38$) to CH_2Cl_2 ($\varepsilon = 8.93$) had little effect on polymerization characteristics (run 10), with only a slight drop of the syndiotacticity to 92% *rr*, due to the enhanced [*mr*] stereodefect (6.1%).

Fourth, we examined the potential anion (i.e., ion-pairing strength) effects by varying activator structures (and thus the resulting anion structure), the results of which are summarized in Table 4. As can be readily seen from the table, the polymerization results with catalysts $\mathbf{6(c,d)}^+[B(C_6F_5)_4]^-$, $\mathbf{6e}^+[B(C_6F_5)_4]^-$, and $\mathbf{6a}^+[MeB(C_6F_5)_3]^-$, derived from the in-reactor activation of the bis(ester enolate) **6** with $[Ph_3C][B(C_6F_5)_4]$ and $[H(OEt_2)_2][B(C_6F_5)_4]$ and activation of the methyl mono(ester enolate) derivative with $THF \cdot B(C_6F_5)_3$, respectively, are remarkably similar in all polymerization aspects (runs 1−3). Polymerization by the catalyst derived from activation with $[Ph_3C]$[TRISPHAT], which introduces the bulky, racemic, *chiral* anion $[TRISPHAT]^-$ to the cation, is somewhat

(29) Busico, V.; Cipullo, R. *Prog. Polym. Sci.* **2001**, *26*, 443–533.

Table 3. Selected Results of MMA Polymerization by Catalyst $\mathbf{6}^{+}[B(C_6F_5)_4]^{-}$

run no.	solvent	temp (°C)	[M]/ [Zr]	time (min)	conv (%)	M_n (10^{-3} g/mol)	PDI (M_w/M_n)	*I** (%)	[*rr*] (%)	[*mr*] (%)	[*mm*] (%)	2[*mm*]/[*mr*]
1	TOL	25	100	4	100	14.7	1.15	70.1	92.8	4.8	2.4	1.00
2	TOL	25	200	10	100	21.9	1.14	92.2	92.8	5.2	2.0	0.77
3	TOL	25	400	45	100	42.2	1.14	95.4	93.7	4.9	1.4	0.57
4	TOL	25	600	60	98.7	60.4	1.16	98.6	93.7	4.8	1.5	0.63
5	TOL	25	800	90	97.4	77.5	1.31	101	94.2	4.6	1.2	0.52
6	TOL	25	1000	120	98.9	71.2	1.32	139	93.5	5.1	1.4	0.55
7	TOL	25	2000	2880	67.5	141	1.53	96.4	94.1	4.4	1.5	0.68
8	TOL	0	400	120	92.4				94.2	4.3	1.5	0.70
9	TOL	50	400	30	91.9				92.9	5.3	1.8	0.68
10	DCM	25	200	30	100	25.7	1.12	78.9	92.1	6.1	1.8	0.59

Table 4. Results of MMA Polymerization with **6** and Different Activators[a]

run no.	catalyst system	time (min)	conv (%)	M_n (10^{-3} g/mol)	PDI (M_w/M_n)	[*rr*] (%)	[*mr*] (%)	[*mm*] (%)
1	$\mathbf{6(c,d)}^{+}[B(C_6F_5)_4]^{-}$	15	97.1	40.0	1.14	93.7	4.9	1.4
2	$\mathbf{6e}^{+}[B(C_6F_5)_4]^{-}$	15	95.3	42.5	1.10	94.6	4.1	1.3
3	$\mathbf{6a}^{+}[MeB(C_6F_5)_3]^{-}$	15	94.6	51.7	1.14	94.6	4.1	1.3
4	$\mathbf{6(c,d)}^{+}$[TRISPHAT]$^{-}$	60	99.3	39.6	1.15	93.2	5.0	1.8

[a] Carried out at 25 °C in 10 mL of toluene + MMA solutions, where $[MMA]_0 = 0.935$ M and $[\mathbf{6}]_0 = [\text{activator}]_0 = 2.34$ mM, for a [MMA]/[catalyst] ratio of 400/1.

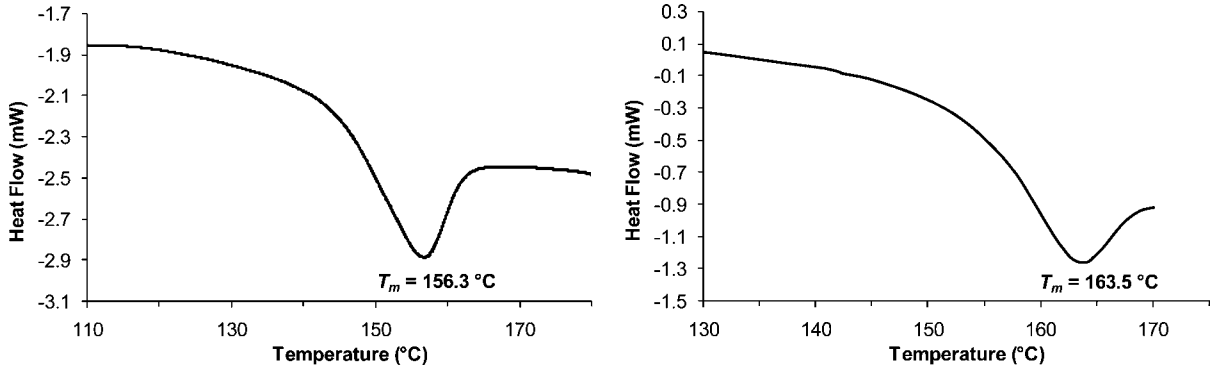

Figure 10. Differential scanning calorimetry traces of *st*-PMMA produced by $\mathbf{6}^{+}[B(C_6F_5)_4]^{-}$ at 25 °C (left, $\Delta H = 6.6$ J/g) and by $\mathbf{4}^{+}[B(C_6F_5)_4]^{-}$ at 0 °C (right, $\Delta H = 4.9$ J/g).

slower (run 4), but it is nonetheless still highly efficient (100% *I**) and syndiospecific (93% *rr*).

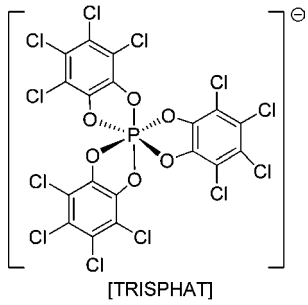

Stereoregulation and Error Formation. In this section we provide a computational rationalization of the experimental observations, especially concerning stereochemical outcomes. Experimentally we observed a high syndiotacticity of 94% *rr* produced by the $Ph_2C<$ bridged catalyst **3**. The calculated ΔE_{stereo} for this catalyst system was 2.3 kcal/mol, which is consistent with the experimental result. The competing transition states for the addition of a MMA molecule to the opposite enantiofaces of the enolate growing chain are shown in Figure 11. Both transition states show a relative *trans* disposition of the methoxy groups of the growing chain and of the monomer. For a complex with an *S* configuration at the metal, the transition state

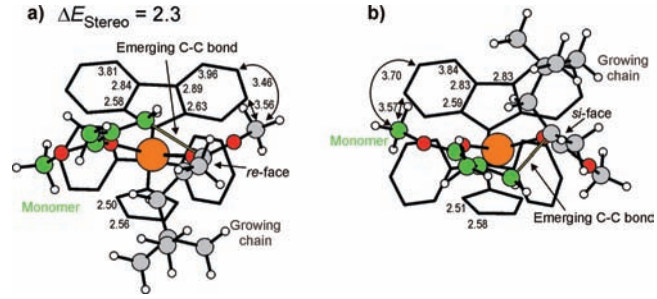

Figure 11. Transition states for MMA addition to the enolate growing chain in $Ph_2C<$ bridged **3** (distances in Å and ΔE_{stereo} in kcal/mol): (a) TS generating a stereomistake; (b) favored TS.

corresponding to MMA attack to the *re*-face of the growing chain is higher and disfavored by steric interaction between the methoxy group of the growing chain and the Flu moiety;[8c] see the short distances in Figure 11a. The preferred transition state for the same *S* complex, which corresponds to MMA attack to the *si*-face of the growing chain, is lower in energy because the methoxy group of the monomer interacts less severely with the Flu moiety (Figure 11b). In both transition states the Flu moiety is pushed toward an η^3-hapticity; see the much larger Zr−C(β) distances relative to the Zr−C(α) distances in the case of the Flu moiety, compared to the rather similar Zr−C(α) and Zr−C(β) distances the in case of the Cp moiety, in Figure 11.

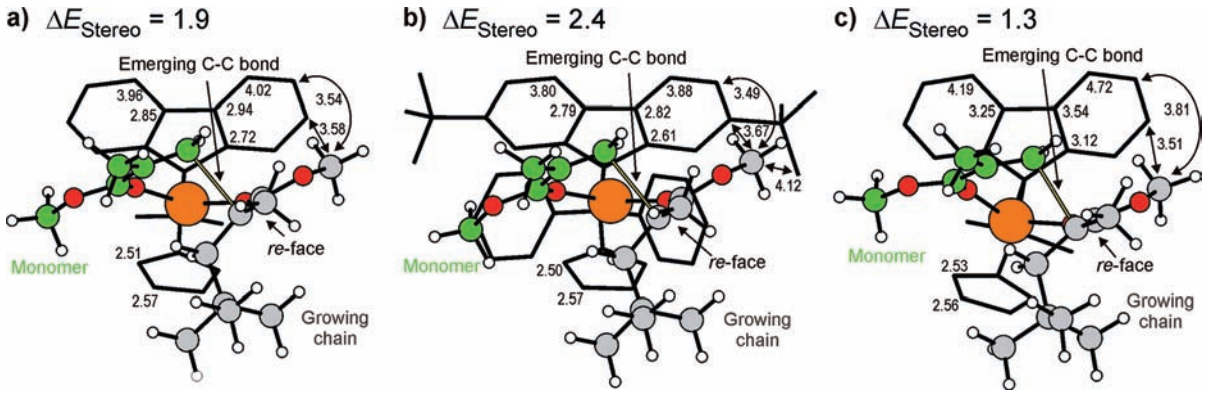

Figure 12. Transition states generating a stereomistake in MMA addition to the enolate growing chain with **2** (a), **6** (b), and **11** (c). Distances in Å and ΔE_{stereo} in kcal/mol.

Scheme 5. Catalyst-Site Epimerization Assisted by MMA after a Stereomistake

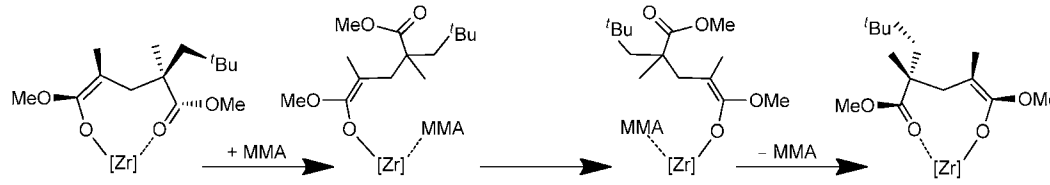

Of course, the syndioregularity of the obtained PMMA can be easily rationalized in the framework of the chain migratory mechanism.

Moving to the $Me_2C<$ bridged catalyst system **2**, replacement of the $Ph_2C<$ bridge with the more flexible $Me_2C<$ bridge results in a small decrease in ΔE_{stereo} by 0.4 kcal/mol relative to that of catalyst **3** (see Figure 12 vs Figure 11). The trend is consistent with the decreased PMMA %*rr* triads on moving from **3** to **2**. It is rather difficult to rationalize this small energy difference, but comparing the two transition states leading to a stereomistake in **2** and **3**, depicted in Figures 11a and 12a, respectively, it is clear that slightly longer distances are found between the methoxy group of the growing chain and the Flu ligand in **2** relative to **3**, which results in a slightly decreased steric stress in **2**. This change can be reasonably ascribed to a higher rigidity of the metallocene skeleton in **3**, a consequence of the bulkier $Ph_2C<$ bridge, which gives rise to a small decrease of the Flu−R_2C−Cp angle on going from **2** (56.7°) to **3** (55.9°). Nevertheless, this small angle decrease results in slightly shorter distances of coordination of the Flu moiety to Zr (compare Figure 11a with Figure 12a). This analysis suggests that the presence of the $Ph_2C<$ bridge pushes the Flu ligand slightly toward the growing chain and the monomer, thereby explaining the higher ΔE_{stereo} calculated for **3**.

Moving to the di-*tert*-butyl-substituted Flu system **6**, introduction of ^{t}Bu groups on the Flu moiety has virtually no effect on ΔE_{stereo}, which is only 0.1 kcal/mol greater than that calculated for **3** (see Figure 12b vs Figure 11a). This value is consistent with the experimentally observed similar amounts of the %*rr* triads in the *st*-PPMA produced by catalyst systems based on **3** and **6**. Visual inspection of the transition states leading to a stereomistake in **3** and **6** rationalizes the minor role of the ^{t}Bu groups in **6**, since these ^{t}Bu groups are more than 4 Å away from the growing chain, while all the other relevant distances are rather similar in **3** and **6**.

Finally, to understand the role of the bridging atom, we focused on system **11**, which corresponds to replacement of the $Ph_2C<$ bridge of **3** with the $Me_2Si<$ bridge. This modification results in a sharp decrease of ΔE_{stereo} by 1.0 kcal/mol (see Figure 12c vs Figure 11a), for a ΔE_{stereo} of only 1.3 kcal/mol, consistent with the poor stereoregularity of the PMMA produced by $R_2Si<$ bridged catalysts relative to the $R_2C<$ analogue. The reason for this rather different behavior can be found in the rather longer Zr−Flu distances in the $Me_2Si<$ bridged **11** relative to $R_2C<$ bridged **2** and **3**. Of course, a slightly looser coordination of the Flu ligand results in an increased distance between the methoxy group of the chain and the Flu ligand (see Figure 12a,c). In the framework of our mechanism, these distances are the *keys* to the transfer of steric stress from the catalyst to the reactants, from which stereoselectivity originates, and longer such distances are consistent with reduced stereoinduction.

Concerning the nature of the stereoerrors (i.e., the relative amount of the *mm* and *mr* triads in the obtained *st*-PPMA), one must recall that, in the framework of a regular chain-migratory mechanism, only *mm* stereoerrors should be observed. Our previous contribution[7a] attributed the high content of *mr* triads of the PMMA produced by CGC systems, apparently consistent with a chain-end stereocontrol, to catalyst-site epimerization occurring after a stereomistake (Scheme 2). The driving force for this site epimerization was related to a different stability of the diastereomeric complexes corresponding to a given (fixed) configuration of the growing chain coupled with the (flexible) configuration at the metal. In fact, calculations indicated that the diastereomeric insertion kinetic product corresponding to the collapse of the transition state yielding a stereomistake was of higher energy relative to that resulting from a correct stereoselectivity. According to our calculations, coordination of a free MMA molecule could assist the epimerization reaction through the intermediates shown in Scheme 5.

The results show that for systems **2**, **3**, and **6**, as in the case of the CGC system, the eight-membered product corresponding

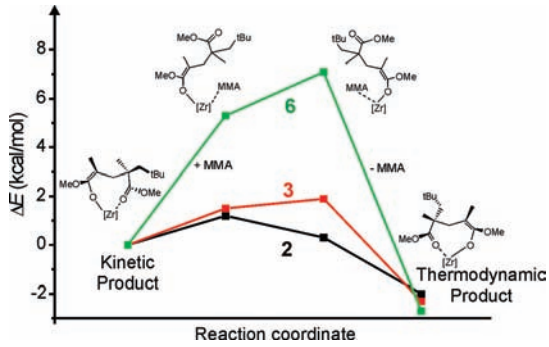

Figure 13. Energy profiles corresponding to the epimerization reaction with systems **2**, **3**, and **6** in CH_2Cl_2.

to the favored transition state (*S*-metal/*si*-chain) is favored relative to the product corresponding to the stereomistake (*S*-metal/*re*-chain; see Figure 13). This result implies that, after a stereomistake has occurred, the eight-membered product has a driving force to epimerize. This driving force originates from steric repulsion between the methoxy group of the growing chain and the Flu moiety that already destabilize the *S*-metal/*re*-chain transition state, as shown in Figures 11 and 12. Indeed, the more stereoselective the catalyst, the larger the energy difference between the eight-membered products corresponding to correct and wrong enantiofacial addition. Nevertheless, the systems show a different propensity to accommodate both the growing chain and an additional MMA molecule at the metal center, namely the intermediate structures in Figure 13. Again, the higher the stereoselectivity, the higher the energy of the intermediates with a coordinated MMA molecule. This trend is particularly evident in the case of the very bulky system **6**. We postulate that the high energy of the intermediates with a coordinated MMA molecule can be related to a slower epimerization rate, which thus should decrease in the order **2** > **3** > **6**. This very simple scheme would rationalize the higher amount of *mr* triads in *st*-PMMA produced by **2** relative to those produced by **3**. In short, the main message here is that lower stereoselectivity and faster epimerization rates correspond to poorly hindered catalysts, because the reactive pockets of these systems have enough space to accommodate both the transition state corresponding to a stereomistake and the intermediates of the epimerization reaction. Even with bulky catalyst **6**, evidence showed that the polymerization at high [MMA]/[catalyst] ratios deviated from a pure site-control mechanism due to higher than expected [*mr*] contents (Table 3), a phenomenon attributable to the herein-described monomer-assisted, catalyst-site epimerization after an enantiofacial mistake.

As described earlier, a propylene-polymerization-like site epimerization followed by a correct MMA addition would also generate the *m*-type stereoerror (Scheme 2). However, in propylene polymerization, site epimerization is a unimolecular process and is favored at low monomer concentration.[18] On the other hand, in MMA polymerization, site epimerization can be either a unimolecular process (by a dissociative pathway, e.g., assisted by the pairing anion or coordinating solvent) or a bimolecular process (assisted by monomer). Our calculations on the CGC catalyst system indicated that the site epimerization assisted by MMA is more facile than that assisted by anion.[7a] Furthermore, our experiments based on the current C_s-ligated catalysts showed a constant syndiotacticity of PMMA produced over a wide polymerization temperature range, insensitivity of its stereoselectivity to solvent polarity and structures of weakly

Scheme 6. Energetics of Back-Biting (E_{BB}) and Ion-Pair Formation (E_{IP}) in **2**, **3**, and **6** in CH_2Cl_2

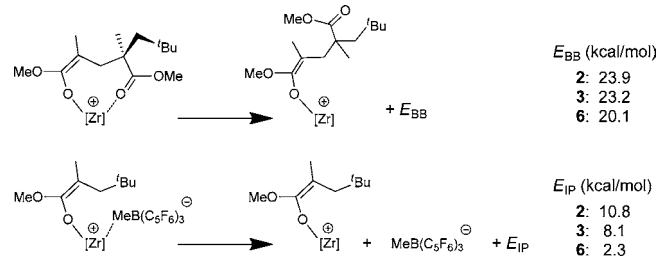

coordinating anions, and deviation from a pure site-control mechanism at high [MMA]/[catalyst] ratios (as opposed to low ratios in the case of propylene polymerization), all of which argue in favor of what we proposed: bimolecular site epimerization involving MMA.

Finally, the energy profiles of Figure 13 suggest that the ability of the various catalysts to coordinate different ligands is quite different, with obvious consequences on their activity. To exploit this point we investigated the energetics of the back-biting of the penultimate unit, E_{BB}, and the energetics of ion-pair formation, E_{IP}, as shown in Scheme 6. The dissociation energy of the C═O group of the last inserted unit in the three representative systems **2**, **3**, and **6** shows a decreasing trend that is in qualitative agreement with the experimental activity, and the same trend is observed for the ion-pair dissociation energy (Scheme 6). Basically, the above-discussed increased rigidity of **3** relative to **2** also results in a reduced ability of **3** to interact with the counterion, as indicated by the E_{IP} of **3** that is 2.7 kcal/mol lower than that of **2**. This effect is much more pronounced for catalyst system **6**, the E_{IP} of which is 5.8 kcal/mol lower than that of **3**. These results suggest that higher activity in these strictly related catalysts can be reasonably related to the ability of the metallocene ligand to prevent tight binding of the bulky counterion.

Conclusions

In summary, this contribution presented a full account of our investigations into the recently discovered catalyst-site-controlled coordination polymerization of polar vinyl monomers into highly syndiotactic polymers. Our combined synthetic, kinetic, mechanistic, and theoretical/computational study has uncovered, and subsequently gained a fundamental understanding of, several unique features of this polymerization system catalyzed by C_s-ligated cationic *ansa*-metallocene ester enolate catalysts.

First, *four* different activation pathways can be employed to convert the precatalyst to the cationic ester enolate catalyst. Methyl mono(ester enolate) precatalysts are best activated with $THF \cdot B(C_6F_5)_3$ at room temperature via methide abstraction, cleanly generating the corresponding cationic ester enolate complexes such as **3** and **6a**$^+[MeB(C_6F_5)_3]^-$. For bis(ester enolate) precatalysts, activation by $B(C_6F_5)_3$ at room temperature affords cleanly the eight-membered chelate **6b**$^+[HB(C_6F_5)_3]^-$ through vinylogous hydride abstraction from the enolate moiety. Activation of the bis(ester enolate) complex with $[Ph_3C][B(C_6F_5)_4]$ at −80 °C gives a mixture of **6c**$^+[B(C_6F_5)_4]^-$ and chelate **6d**$^+[B(C_6F_5)_4]^-$ as a result of electrophilic addition of Ph_3C^+ to the enolate and of vinylogous hydride abstraction of the enolate group by Ph_3C^+, respectively. Although **6c**$^+[B(C_6F_5)_4]^-$ is stable only at low temperatures, in the presence of monomer it can be rapidly converted to the resting chelate **6d**$^+[B(C_6F_5)_4]^-$; this feature ensures the success seen

for the in-reactor activation methodology operating at low, ambient, or higher temperatures. The protonolysis approach involves the cleavage of the Zr−enolate bond with $[H(Et_2O)_2][B(C_6F_5)_4]$, which occurs instantaneously even at −80 °C, cleanly generating the cationic ester enolate **6e**$^+[B(C_6F_5)_4]^-$. This structure simulates the catalyst−monomer complex in a propagation catalysis cycle and is stable only at low temperatures; however, we can "watch" it consume MMA, leading to the eight-membered chelate **6f**$^+[B(C_6F_5)_4]^-$ and subsequent PMMA formation.

Second, among the 12 catalyst systems we examined in this study—which varied in metal center, anion structure, bridging atom and substituents, and ligand substitution pattern—the $Ph_2C<$ bridged, di-*tert*-butyl-substituted Flu catalyst system **6**, by in-reactor activation with $[Ph_3C][B(C_6F_5)_4]$ at room temperature, is the best in *all* aspects of the polymerization, having the highest observed activity (1554 h^{-1} TOF), efficiency (98% *I**), syndiotacticity (94% *rr*), and control (predicted M_n and 1.14 MWD). This catalyst system is also remarkably robust, producing highly syndiotactic PMMA with a constant syndiotacticity over a wide polymerization temperature range, from 0 °C, 94% *rr* to 25 °C, 94% *rr* to 50 °C, 93% *rr*. Its polymerization characteristics are insensitive to solvent polarity. Such temperature and solvent insensitivities are in marked contrast to the propylene polymerization by analogous C_s-ligated cationic alkyl catalysts. Additionally, the polymerization characteristics of catalyst system **6** are insensitive to anion structure of weekly coordinating anions, such as $[MeB(C_6F_5)_3]^-$, $[B(C_6F_5)_4]^-$, and $[TRISPHAT]^-$. Furthermore, this cationic catalyst is soluble in toluene, adding an additional advantage to the polymerization process.

Third, kinetic experiments show that MMA polymerization by **6**$^+[B(C_6F_5)_4]^-$ in toluene at room temperature follows first-order kinetics in both monomer and catalyst concentrations, consistent with a monometallic, intramolecular coordination−addition mechanism. Other mechanistic insights gained from examining fundamental reaction steps and polymerization processes provide collaborative evidence to support this mechanism that involves in the propagation "catalysis" cycle the fast intramolecular Michael addition within the catalyst−monomer complex, leading to the resting eight-membered ester enolate chelate, followed by the slower, rate-limiting ring-opening of the chelate to regenerate the active species.

Fourth, on the theoretical side, DFT calculations rationalized why the $Ph_2C<$ bridged catalyst system **6** exhibits higher stereoselectivity than **2** (with the $Me_2C<$ bridge) or **11** (with the $Me_2Si<$ bridge). Installation of the bulky $Ph_2C<$ bridge decreases the Flu−C−Cp angle and thus pushes the η^3-bound Flu ligand closer to the growing chain and the monomer, thereby increasing ΔE_{stereo} between the competing transition states for the addition of a MMA molecule to the opposite (correct and wrong) enantiofaces of the growing enolate chain. Computational results also provided theoretical explanations for the observed deviation from a pure site-control mechanism at high [MMA]/[catalyst] ratios due to higher than expected [*mr*] contents, a phenomenon attributable to the herein-described monomer-assisted, catalyst-site epimerization, after an enantiofacial mistake, to a thermodynamically more stable resting state. Furthermore, the relative polymerization activity of this strictly related catalyst series was shown to correlate with the relative energetics of the back-biting of the penultimate unit and ion-pair formation.

Finally, on the basis of what we have learned so far and in the interest of creating more active, efficient, and stereoselective C_s-ligated catalysts for coordination polymerization of polar vinyl monomers, future efforts should perhaps be directed at designing catalyst structures that can provide higher rigidity of the C_s-metallocene skeleton, achievable by using appropriate bridging atoms and associated substituents as well as substitutions at suitable positions of the Flu ring. An ideal outcome should be a balanced stereo-interplay between the catalyst and the reactant for both high reactivity and stereoselectivity. Stronger coordination of the Flu ligand should more effectively transfer steric stress from the catalyst site to the reactants. Research toward these directions is currently underway.

Acknowledgment. This work was supported by the National Science Foundation (NSF-0718061) for the work carried out at Colorado State University and by INSTM (Cineca Grant Key Project) for the work carried out at the University of Salerno. L. Cavallo thanks the HPC team of Enea (www.enea.it) for use of the ENEA-GRID and the HPC facilities CRESCO (www.cresco.enea.it) in Portici, Italy. We thank Susie Miller for help with the X-ray diffraction analyses of complexes **7** and **11**, and Boulder Scientific Co. for the research gifts of $B(C_6F_5)_3$, $[Ph_3C][B(C_6F_5)_4]$, and $[Ph_2C(Cp)(Flu)]ZrCl_2$.

Supporting Information Available: Experimental details and crystallographic data for **7** and **11** (CIF). This material is available free of charge via the Internet at http://pubs.acs.org.

JA908818Y